THE JOURNAL OF PHYSICAL CHEMISTRY C

ARTICLE

pubs.acs.org/JPCC

Effect of Thermoelectric Cooling in Nanoscale Junctions

Yu-Shen Liu, Bailey C. Hsu, and Yu-Chang Chen*

Department of Electrophysics, National Chiao Tung University, 1001 Ta Hsueh Road, Hsinchu 30010, Taiwan

ABSTRACT: We propose a thermoelectric cooling device based on an atomic-sized junction. Using first-principles approaches, we investigate the working conditions and the coefficient of performance (COP) of an atomic-scale electronic refrigerator where the effects of the phonon's thermal current and local heating are included. It is observed that the functioning of the thermoelectric nanorefrigerator is restricted to a narrow range of driving voltages. Compared with the bulk thermoelectric system with the overwhelmingly irreversible Joule heating, the 4-Al atomic refrigerator has a higher efficiency than a bulk thermoelectric refrigerator with the same thermoelectric figure of merit (ZT) due to suppressed local heating via the quasi-ballistic electron transport and small driving voltages. Quantum nature due to the size minimization offered by atomic-level control of properties facilitates electron cooling beyond the expectation of the conventional thermoelectric device theory.

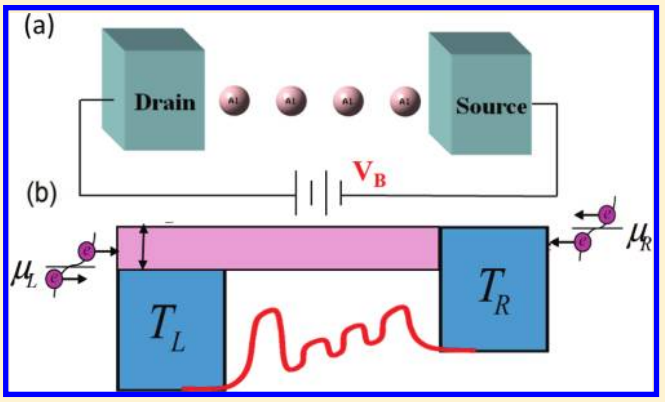

I. INTRODUCTION

The miniaturization of devices has been eliciting a tremendous wave of multidisciplinary scientific interest.[1,2] This interest is motivated by the aspiration to develop new forms of electronic devices based on nanostructures. To develop the nanodevices at the atomic/molecular level, understanding of nonequilibrium quantum transport theory is of critical importance. In the past decade, a growing number of studies have been conducted to diversify the scopes of molecular electronics including the current−voltage characteristics,[3−7] inelastic electron tunneling spectroscopy (IETS),[8−16] shot noise,[17−20] counting statistics,[21] local heating,[22,24] and gate-controlled effect.[25−29] Substantial progress has been achieved in experiments and theories.[30−32]

Recently, atomic/molecular thermoelectric junctions are gaining increased attention due to the recent measurements of the Seebeck coefficient, defined as $S = dV/dT$, where dV is the voltage difference caused by the temperature difference dT by the Seebeck effect.[33−36] Measurements of the Seebeck coefficient provide a useful experimental approach to exploring the electronic structure of the molecule bridging the electrodes.[37] Methodologically, the scope of the research needs to extend through the utilization of unprecedented experiments. These experiments inspire rapid development in the theory of thermoelectricity at the atomic and molecular scale including the Seebeck coefficients, thermoelectric figure of merit (ZT), thermospin effect, and effect of electron−phonon interactions.[38−52]

The effect of thermoelectricity hybridizes the interactions between electron and energy transport under nonequilibrium conditions. In the bulk and mesoscopic systems, the efficiency of a thermoelectric (TE) refrigerator is usually suppressed by a large work function. For example, the operation of a thermoelectric cooling device such as a vacuum diode is limited to very high temperatures (T_{op} > 1000 K) due to its large potential barrier.[53] Another pronounced drawback in the bulk system is the overwhelmingly irreversible Joule heating due to diffused electrons which significantly suppresses the efficiency of thermoelectric refrigerators. Recently, researchers have looked into creating thermoelectric refrigerators that operate at room temperatures. For this purpose, semiconductor heterostructures have been proposed to reduce the work function.[54−57] A new solution to the low-temperature-operated thermoelectric refrigerators may be the atomic-sized junctions, the extreme limit of device miniaturization.

The atomic-sized energy-conversion devices have gained growing interest in material science and nanoscience. The electron transport mechanism in these systems is characterized by quasi-ballistic electron transport due to the small size. Previous reports thus far have mainly focused on the Seebeck coefficient (S) and the thermoelectric figure of merit (ZT) of nanojunctions. Several attempts have been made to understand the cooling mechanism in nanojunctions.[58−63] This study proposes a thermoelectric cooling device based on an atomic junction. This project develops a theory of the atomic-scale cooling mechanism for quasi-ballistic electrons under nonequilibrium conditions from first-principles approaches. We investigate the nanorefrigerator's working conditions, the electron's thermal current which removes heat from the cold-temperature reservoir, and the coefficient of performance (COP) in the presence of the phonon's thermal current and local heating. We observe that the potential barrier is effectively suppressed by

Received: November 15, 2010
Revised: February 6, 2011
Published: March 08, 2011

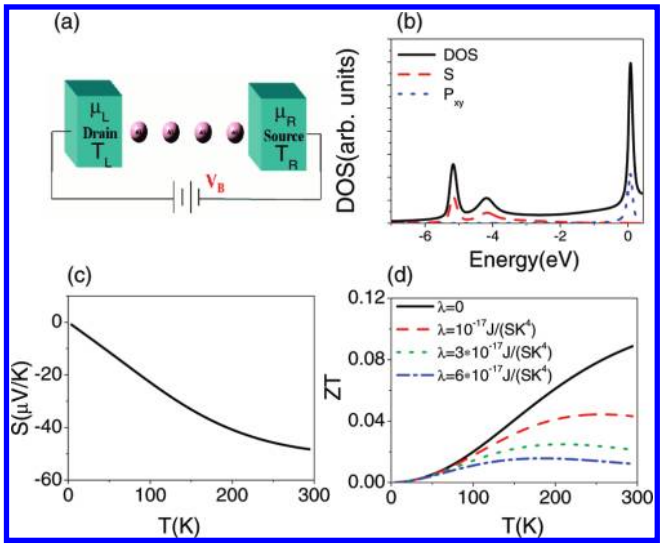

Figure 1. (a) Scheme of the 4-Al atomic junction with different temperatures $T_{L(R)}$ and chemical potentials $\mu_{L(R)}$. The Al−jellium distance is about 2.5 au, and the Al−Al bond distance is about 6.3 au. (b) Density of state and projected density of states of the 4-Al junction. (c) Seebeck coefficient vs temperature of the 4-Al junction, and (d) ZT vs T with the phonon's thermal current for various values of λ.

the resonant tunneling and that the local heating is significantly suppressed by the reduced dimension. Nanorefrigerators with a figure of merit comparable to conventional TE refrigerators usually have better coefficient of performance, taking advantage of the reduced local heating due to the small size. These quantum features remarkably facilitate the electron cooling in nanoscale thermoelectric refrigerators beyond the expectation of the conventional bulk thermoelectric device theory.

As an example, we consider an ideal 4-Al monatomic junction, as depicted in Figure 1(a). The Seebeck coefficient of the 4-Al atomic junction is characterized by a larger Seebeck coefficient induced by a sigma channel near the chemical potentials with the P_x-P_y orbital characters. Due to the small size, local heating and photon radiation are sufficiently suppressed that they can be safely neglected compared with the large phonon's thermal current considered in this study. Calculations indicate that the 4-Al junction is able to work at temperatures below 100 K. Compared with atomic-scale thermoelectric power generators,[64,65] thermoelectric nanorefrigerators require more stringent working conditions. For example, we observe that the battery which drives the thermoelectric nanorefrigerator is restricted to a range of voltages between the lower and upper threshold biases.

The flow of the discussion in this paper is as follows. First, we describe the details of density functional theory, theory of thermoelectricity, and theory of thermoelectric nanorefrigerator without and with the phonon's thermal current and local heating in Section II. In Section III, we discuss the thermoelectric properties of 4-Al atomic junctions and subsequently discuss the onset bias, working conditions, and COP of thermoelectric nanorefrigerators. We then summarize our findings in Section IV.

II. THEORETICAL METHODS

The theory presented in the following is general to any atomic/molecular junction characterized by the quasi-ballistic transport. In Section II. A, Density Functional Theory, we present an introduction of the density functional theory (DFT). In Section II. B, Theory of Thermoelectricity, we present the theory to calculate the Seebeck coefficient, electric conductance, electron's thermal conductance, phonon's thermal conductance, and thermoelectric figure of merit (ZT). In Section II. C, Theory of Thermoelectric Refrigerator, we present the theory for electronic cooling without and with the phonon's thermal current and local heating.

II. A. Density Functional Theory. We present a brief introduction of how to calculate the electric current and the electron's thermal current in the DFT framework. We picture a nanoscale junction as formed by two semi-infinite electrodes held apart at a fixed distance with a nanostructured object bridging the gap between them. The full Hamiltonian of the system is $H = H_0 + V$, wherein H_0 is the Hamiltonian due to the bare electrodes and V is the scattering potential of the nanostructured object.

First, we calculate the wave functions of the bare electrodes with an applied bias $V_B = (\mu_R - \mu_L)/e$, where $\mu_{L(R)}$ is the chemical potential deep in the left (right) electrode. The unperturbed wave functions of the bare electrodes have the form, $\Psi^{0,L(R)}_{E\mathbf{K}_\parallel}(\mathbf{r}) = e^{i\mathbf{k}_\parallel\cdot\mathbf{R}}\cdot u^{L(R)}_{E\mathbf{K}_\parallel}(z)$, where $u^{L(R)}_{E\mathbf{K}_\parallel}(z)$ describes the electrons incident from the left (right) electrode before the inclusion of the nanostructured object. The wave function $u^{L(R)}_{E\mathbf{K}_\parallel}(z)$ is calculated by solving the Shrödinger equation and Poisson equations iteratively until self-consistency is obtained. Note that $u^{R}_{E\mathbf{K}_\parallel}(z)$ satisfies the following boundary condition

$$u^{R}_{E\mathbf{K}_\parallel}(z) = (2\pi)^{-3/2}\times\begin{cases}\dfrac{1}{\sqrt{k_R}}(e^{-ik_Rz}+Re^{ik_Rz}), z\to\infty\\ \dfrac{1}{\sqrt{k_L}}Te^{-ik_Lz}, z\to-\infty\end{cases} \quad (1)$$

where $\mathbf{K}_\parallel$ is the electron momentum in the plane parallel to the electrode surfaces, and z is the coordinate parallel to the direction of the current. The condition of energy conservation gives $(1/2)k_R^2 = E - (1/2)|\mathbf{K}_\parallel|^2 - v_{eff}(\infty)$ and $(1/2)k_L^2 = E - (1/2)|\mathbf{K}_\parallel|^2 - v_{eff}(-\infty)$, where $v_{eff}(z)$ is the effective potential comprising the electrostatic and exchange-correlation potentials.

The nanostructured object is considered as a scattering center. The scattering wave functions of the entire system are calculated by solving the Lippmann−Schwinger equation in the scattering approaches iteratively until self-consistency is obtained

$$\Psi^{L(R)}_{E\mathbf{K}_\parallel}(\mathbf{r}) = \Psi^{0,L(R)}_{E\mathbf{K}_\parallel}(\mathbf{r}) + \int d^3\mathbf{r}_1\int d^3\mathbf{r}_2 G^0_E(\mathbf{r},\mathbf{r}_1)V(\mathbf{r}_1,\mathbf{r}_2)\Psi^{L(R)}_{E\mathbf{K}_\parallel}(\mathbf{r}_2) \quad (2)$$

where $\Psi^{L(R)}_{E\mathbf{K}_\parallel}(\mathbf{r})$ stands for the effective single-particle wave functions of the entire system, which also represents the electrons with energy E incident from the left (right) electrode. The potential $V(\mathbf{r}_1,\mathbf{r}_2)$ that the electrons experience when they scatter through the nanojunction is

$$V(\mathbf{r}_1,\mathbf{r}_2) = V_{ps}(\mathbf{r}_1,\mathbf{r}_2) + \left\{(V_{xc}[n(\mathbf{r}_1)] - V_{xc}[n_0(\mathbf{r}_1)]) + \int d\mathbf{r}_3\frac{\delta n(\mathbf{r}_3)}{|\mathbf{r}_1-\mathbf{r}_3|}\right\}\delta(\mathbf{r}_1-\mathbf{r}_2) \quad (3)$$

where $V_{ps}(\mathbf{r}_1,\mathbf{r}_2)$ is the electron−ion interaction potential represented with pseudopotential; $V_{xc}[n(\mathbf{r})]$ is the exchange-correlation potential calculated at the level of the local-density

approximation; $n_0(\mathbf{r})$ is the electron density for the pair of biased bare electrodes; $n(\mathbf{r})$ is the electron density for the total system; and $\delta n(\mathbf{r})$ is their difference. The quantity G_E^0 is the Green's function for the bare electrodes. The wave functions that achieve self-consistency in the DFT framework in plane wave basis are applied to calculate the electric current and the electron's thermal current.

These right- and left-moving wave functions weighed with the Fermi−Dirac distribution function according to their energies and temperatures are applied to calculate the electric current as

$$I(\mu_L, T_L; \mu_R, T_R) = \frac{e\hbar}{mi}\int dE \int d\mathbf{r}_\perp \times \int d\mathbf{K}_\parallel [f_E(\mu_R, T_R) I^{RR}_{EE,\mathbf{K}_\parallel}(\mathbf{r}) - f_E(\mu_L, T_L) I^{LL}_{EE,\mathbf{K}_\parallel}(\mathbf{r})] \quad (4)$$

where $I^{RR(LL)}_{EE',\mathbf{K}_\parallel}(\mathbf{r}) = [\Psi^{R(L)}_{E,\mathbf{K}_\parallel}(\mathbf{r})]^* \nabla \Psi^{R(L)}_{E',\mathbf{K}_\parallel}(\mathbf{r}) - \nabla[\Psi^{R(L)}_{E,\mathbf{K}_\parallel}(\mathbf{r})]^* \Psi^{R(L)}_{E',\mathbf{K}_\parallel}(\mathbf{r})$ and $d\mathbf{r}_\perp$ represents an element of the electrode surface. Here, we assume that the left and right electrodes are independent electron reservoirs, with the population of the electron described by the Fermi−Dirac distribution function, $f_E(\mu_{L(R)},T_{L(R)}) = 1/\{\exp[(E-\mu_{L(R)})/(k_B T_{L(R)})] + 1\}$, where $\mu_{L(R)}$ and $T_{L(R)}$ are the chemical potential and the temperature in the left (right) electrode, respectively. More detailed descriptions of theory can be found in refs 4, 73, and 74.

The above expression can be cast in a Landauer−Büttiker formalism

$$I(\mu_L, T_L; \mu_R, T_R) = \frac{2e}{h}\int dE \tau(E)[f_E(\mu_R, T_R) - f_E(\mu_L, T_L)] \quad (5)$$

where $\tau(E) = \tau^R(E) = \tau^L(E)$ is a direct consequence of the time-reversal symmetry, and $\tau^{R(L)}(E)$ is the transmission function of the electrons with energy E incident from the right (left) electrode

$$\tau^{R(L)}(E) = \frac{\pi\hbar^2}{mi}\int d\mathbf{r}_\perp \int d\mathbf{K}_\parallel I^{RR(LL)}_{EE,\mathbf{K}_\parallel}(\mathbf{r}) \quad (6)$$

There is an analog between the electric current and the electron's thermal current. The flow of electrons can also transport energy. The electron's thermal current, defined as the rate at which thermal energy flows from the right (into the left) electrode, is

$$J^{R(L)}_{el}(\mu_L, T_L; \mu_R, T_R) = \frac{2}{h}\int dE(E-\mu_{R(L)})\tau(E)[f_E(\mu_R, T_R) - f_E(\mu_L, T_L)] \quad (7)$$

II. B. Theory of Thermoelectricity. Here, we present the theory to calculate the zero-bias electric conductance, Seebeck coefficient, and electron's thermal conductance for a thermoelectric nanojunction in terms of the effective single-particle wave functions obtained self-consistently within the static density functional theory in a truly atomic-scale junction.

We assume that the left and right electrodes serve as independent temperature reservoirs. The population of electrons in the left (right) electrode is described by the Fermi−Dirac distribution function, $f_E(\mu_{L(R)},T_{L(R)}) = 1/\{\exp[(E-\mu_{L(R)})/(k_B T_{L(R)})] + 1\}$, where the chemical potentials are $\mu_R = \mu_L = \mu$ (i.e., at zero external bias). Let us now consider an extra infinitesimal current induced by an additional infinitesimal temperature (dT) and voltage (dV) across the junctions in an open circuit. The currents induced by dT and dV are $(dI)_T = I(\mu,T;\mu,T+dT)$ and $(dI)_V = I(\mu,T;\mu+dV,T)$, respectively, where $I(\mu,T;\mu,T+dT)$ and $I(\mu,T;\mu,T+dT)$ are given by eq 5. Suppose that the current cannot actually flow in an open circuit, thus $(dI)_T$ counterbalances $(dI)_V$. In other words, the extra net current is zero

$$dI = I(\mu, T; \mu + edV, T + dT) \approx (dI)_T + (dI)_V = 0 \quad (8)$$

The Fermi−Dirac distribution function in eq 8 can be expanded up to the first order in dT and dV, and we obtain the Seebeck coefficient (defined by $S = dV/dT$)

$$S(\mu, T) = -\frac{1}{eT}\frac{K_1(\mu, T)}{K_0(\mu, T)} \quad (9)$$

where

$$K_n(\mu, T) = -\int dE\tau(E)(E-\mu)^n \frac{\partial f_E(\mu, T)}{\partial E} \quad (10)$$

The Seebeck coefficient in the low-temperature regime can be obtained by expanding $K_n(\mu,T)$ to the lowest order in temperature through the Sommerfeld expansion, that is, $K_0 \approx \tau(\mu)$, $K_1 \approx [\pi^2 k_B^2 \tau'(\mu)/3]T^2$, and $K_2 \approx [\pi^2 k_B^2 \tau(\mu)/3]T^2$. The Seebeck coefficient up to the lowest order in temperature is

$$S \approx \alpha T \quad (11)$$

where $\alpha = -[\pi^2 k_B^2(\partial\tau(\mu))/(\partial E)]/(3e\tau(\mu))$. The Seebeck coefficient is positive (negative) when the slope of transmission function is negative (positive), which is closely related to the transmission function near the chemical potentials. We note that the Seebeck coefficient can be optimized via the gate voltage which shifts the DOSs.

The electron's thermal current is the energy current carried by electrons traveling between electrodes driven by dT and dV. Analogous to the extra current given by eq 8, the extra electron's thermal current is

$$dJ_{el} = (dJ_{el})_T + (dJ_{el})_V \quad (12)$$

where $(dJ_{el})_T = J_{el}(\mu,T;\mu,T+dT)$ and $(dJ_{el})_V = J_{el}(\mu,T;\mu+edV,T)$ are the fractions of electron's thermal current driven by dT and dV, respectively. Note that dV is generated by the Seebeck effect according to the temperature difference dT. Both $J_{el}(\mu,T;\mu,T+dT)$ and $J_{el}(\mu,T;\mu+edV,T)$ can be calculated using eq 7.

Given that we define the electron's thermal conductance as $k_{el} = dJ_{el}/dT$, the electron's thermal conductance k_{el} can decompose into two components

$$\kappa_{el}(\mu, T) = \kappa^T_{el}(\mu, T) + \kappa^V_{el}(\mu, T) \quad (13)$$

where $\kappa^T_{el} = (dJ_{el})_T/dT$ and $\kappa^V_{el} = (dJ_{el})_V/dT$. We note that κ^T_{el} and κ^V_{el} are the portions of the electron's thermal conductance driven by dT and dV, respectively. Analogous to eq 9, κ^T_{el} and κ^V_{el} can be can be expressed by eq 10

$$\kappa^T_{el}(\mu, T) = \frac{2}{h}\frac{K_2(\mu, T)}{T} \quad (14)$$

and

$$\kappa^V_{el}(\mu, T) = \frac{2e}{h}K_1(\mu, T)S(\mu, T) \quad (15)$$

dx.doi.org/10.1021/jp110920q |J. Phys. Chem. C 2011, 115, 6111–6125

One should note that $\kappa_{el}^V = 0$ if the Seebeck coefficient of the system is zero because dV is zero.

In the low-temperature regime, κ_{el}^T and κ_{el}^V can be expanded to the lowest order in temperatures using the Sommerfeld expansion

$$\kappa_{el}^V \approx \beta_V T^3 \text{ and } \kappa_{el}^T \approx \beta_T T \tag{16}$$

where $\beta_V = -2\pi^4 k_B^4[\tau'(\mu)]^2/(9h\tau(\mu))$ and $\beta_T = 2\pi^2 k_B^2 \tau(\mu)/(3h)$. In the above expansions, we also applied the following approximations: $K_1(\mu,T) \approx \pi^2 k_B^2 \tau'(\mu)/3]T^2$, $K_2(\mu,T) \approx \pi^2 k_B^2 \tau(\mu)/3]T^2$, and eq 11. In the low-temperature regime, κ_{el}^T dominates the electron's thermal current. Thus, $\kappa_{el} \approx \kappa_{el}^T$ is linear in T; that is

$$\kappa_{el}(\mu, T) \approx \beta_T T \tag{17}$$

At zero bias, the electric conductance can be expressed as

$$\sigma(T) = \frac{2e^2}{h}\int dE f_E(\mu, T)[1 - f_E(\mu, T)]\tau(E)/(k_B T) \tag{18}$$

In the low-temperature regime, the zero-bias conductance is usually insensitive to temperatures if tunneling is the major transport mechanism.

Thus far, the physical quantities (S, σ, and κ_{el}) previously discussed are related to the propagation of electrons. The heat current carried by the phonon may occur in a real system. The phonon's thermal current, which is driven by the temperature difference ΔT, flows from the hot reservoir into the cold reservoir. To determine the impact of the phonon's thermal current on refrigeration, the weak link model is chosen to describe it. The weak link model assumes that the nanojunction is a weak elastic link with a given stiffness K that can be evaluated from total energy calculations or from experimental measurement.[68] Two metal electrodes are regarded as the macroscopic bodies under their thermodynamic equilibrium and are taken as ideal thermal conductors. To the leading order in the strength of the weak link, the phonon's thermal current (J_{ph}) via elastic phonon scattering is[68]

$$J_{ph} = \frac{2\pi K^2}{\hbar}\int_0^\infty dE E N_L(E) N_R(E)[n_L(E) - n_R(E)] \tag{19}$$

where K is the stiffness of the weak elastic link; $N_{L(R)}(E)$ is the spectral density of phonon states at the left (right) electrode surface which is measurable by experiments; and $n_{L(R)} \equiv 1/(e^{E/K_B T_{L(R)}} - 1)$ is the Bose−Einstein distribution function. In the long wavelength limit, the spectral density of surface phonon is given by $N_{L(R)}(E) \approx CE$. The phonon's thermal conductance defined as $\kappa_{ph} = \Delta J_{ph}/\Delta T$ as $\Delta T \to 0$ is

$$\kappa_{ph} = \left[J_{ph}\left(T_L + \frac{\Delta T}{2}, T_R - \frac{\Delta T}{2}\right) - J_{ph}(T_L, T_R)\right]/\Delta T \tag{20}$$

Expanding the Bose−Einstein distribution function in $J_{ph}(T_L + (\Delta T/2), T_R - (\Delta T/2))$ to the first order of ΔT, we obtain the phonon's thermal conductance

$$\kappa_{ph} = \frac{\pi K^2 C^2}{\hbar}\int_0^\infty dE E^3 \sum_{i=L,R} \frac{\partial n_i(E)}{\partial T_i} \tag{21}$$

When $T_R \approx T_L = T$, then eq 21 is reduced to

$$\kappa_{ph} = \frac{2\pi K^2 C^2}{\hbar}\int_0^\infty dE E^3 \frac{\partial n(E)}{\partial T} \tag{22}$$

where $n = 1/[e^{E/(k_B T)} - 1]$.

The efficiency of thermoelectric nanodevices is conventionally described by the thermoelectric figure of merit ZT, which depends on the following physical factors: Seebeck coefficient (S), electric conductance (σ), electron's thermal conductance (κ_{el}), and phonon's thermal conductance (κ_{ph}). ZT is defined as

$$ZT = \frac{S^2\sigma}{\kappa_{el} + \kappa_{ph}} T \tag{23}$$

where S, σ, κ_{el}, and κ_{ph} can be numerically calculated using eqs 9, 18, 13, and 22, respectively. When ZT tends to infinity, the thermoelectric efficiency of nanojunctions will reach Carnot efficiency.

II. C. Theory of the Thermoelectric Refrigerator. Now, we present the theory of a thermoelectric cooling device at atomic scale including the effect of the phonon's thermal current and local heating. We assume that the left (right) electrode serves as the hot (cold) temperature reservoir with temperature $T_R = T_C$ ($T_L = T_H = T_C + \Delta T$), and the phonon's population is described by the Bose−Einstein distribution function. We consider the nanojunction connecting to an external battery with bias $V_B = (\mu_R - \mu_L)/e$, which drives the electrons flowing from the right to left electrodes. The thermal current carried by electrons traveling between two electrodes is given by eq 7. It should be noted that

$$\begin{aligned} &J_{el}^R(\mu_L, T_L; \mu_R, T_R) + I(\mu_L, T_L; \mu_R, T_R)V_B \\ &\quad = J_{el}^L(\mu_L, T_L; \mu_R, T_R) \end{aligned} \tag{24}$$

where $I(\mu_L,T_L;\mu_R,T_R)$ is the current given by eq 5. Equation 24 states that the energy is conserved: it consumes electric energy to take heat from the right (cold) into the left (hot) reservoir. Thus, the thermoelectric junction can be regarded as an electronic cooling device when $J_{el}^R > 0$, which states that the thermoelectric junction is capable of removing heat from the cold reservoir.

A measure of a refrigerator's performance is the ratio of the rate of heat removed from the cold reservoir to the electric power done on the system. The ratio is called the coefficient of performance (COP)

$$\eta_{el} = \frac{J_{el}^R}{IV_B} = \frac{J_{el}^R}{|J_{el}^R - J_{el}^L|} \tag{25}$$

where V_B is the bias applied across the nanojunction driving the thermoelectric refrigerator; I is the electric current; and J_{el}^R is the rate of thermal energy removed from the cold reservoir. The thermoelectric junction as a nanorefrigerator is working when $J_{el}^R > 0$ (and thus $\eta > 0$).

II. C. 1. Properties of Thermoelectric Refrigerator in the Absence of the Phonon's Thermal Current. In the following, we develop an analytical theory to gain insight into the fundamentals of the cooling effect in the thermoelectric nanojunction. We apply the Sommerfeld expansion to $J_{el}^R(\mu_L,T_L;\mu_R,T_R)$ and obtain

$$\begin{aligned} J_{el}^R \approx &\frac{\pi^2 k_B^2}{3h}[\tau(\mu_L)(T_R^2 - T_L^2) + \tau'(\mu_L)(\mu_R - \mu_L)(T_R^2 + T_L^2)] \\ &- \frac{1}{h}[\tau(\mu_L)(\mu_R - \mu_L)^2] - \frac{1}{3h}[\tau'(\mu_L)(\mu_R - \mu_L)^3] \end{aligned} \tag{26}$$

where we use the following relations: $\tau(E) \approx \tau(\mu_L) + \tau'(\mu_L)(E - \mu_L)$, $\tau(\mu_R) \approx \tau(\mu_L) + \tau'(\mu_L)(\mu_R - \mu_L)$, $T_L = T_R + \Delta T$, $\int_{\mu_L}^{\mu_R}(E - \mu_R)dE = -(1/2)(\mu_R - \mu_L)^2$, $\int_{\mu_L}^{\mu_R}(E - \mu_L)(E - \mu_R)dE = -(1/6)(\mu_R - \mu_L)^3$, and $\mu_R - \mu_L = eV_B$. When $\Delta T \ll T_R$, eq 26 can be expressed as a polynomial of V_B

$$J_{el}^{R} = -a + bV_B - cV_B^2 - dV_B^3 \tag{27}$$

where $a = 2\pi^2 k_B^2 \tau(\mu) T_R \Delta T/(3h)$, $b = 2e\pi^2 k_B^2 \tau'(\mu) T_R{}^2/(3h)$, $c = e^2\tau(\mu)/h$, and $d = e^3\tau'(\mu)/(3h)$. The above equation is convenient for analytical exploration of the properties of thermoelectric nanorefrigerators.

A thermoelectric nanorefrigerator functions only when the maximum value of the electron's thermal current is positive, that is, $(J_{el}^{R})_{max} > 0$. In a small bias regime, the term $V_B{}^3$ can be neglected in eq 27, i.e., $J_{el}^{R} \approx -a + bV_B - cV_B^2$. In this case, the working condition of the nanorefrigerator is given by $(J_{el}^{R})_{max} = (-4ac + b^2)/(4c) > 0$, which yields the criterion for the existence of electronic cooling

$$-S > \sqrt{\frac{2\pi^2 k_B^2}{3e^2}\left(\frac{\Delta T}{T_R}\right)} \tag{28}$$

where $S = -[(\pi^2 k_B^2)/(3e)][\tau'(\mu)/\tau(\mu)]T_R$ is the Seebeck coefficient of the nanoscale junction.[50]

For a given T_R and a given temperature difference ΔT, $J_{el}^{R}(V_B)$ is a function of bias V_B. We observe that J_{el}^{R} is negative at $V_B = 0$, and thus a lower limit of bias (denoted as $V_{el}^{th,lower}$) is needed. The lower threshold bias is defined as the smallest positive solution of $J_{el}{}^{R}(V_B) = 0$. For $V_B < V_{el}^{th,lower}$, $J_{el}^{R} < 0$ and the thermoelectric cooling effect does not exist. Moreover, it is observed that there is an upper bound of bias for the operation of the thermoelectric nanorefrigerator. To show this, we keep the terms up to $O(V_B^2)$ in eq 27, i.e., $J_{el}^{R}(V_B) \approx -a + bV_B - cV_B^2$. In this simple case, the lower threshold bias $V_{el}^{th,lower}$ and the upper threshold bias $V_{el}^{th,upper}$ are derived from $J_{el}^{R}(V_B) = 0$, from which we obtain the lower and upper bounds of the working biases

$$V_{el}^{th,lower} \approx -\frac{\pi^2 k_B^2 \Delta T}{3e^2 S T_R} \tag{29}$$

and

$$V_{el}^{th,upper} \approx 2ST_R^2 - V_{th}^{el} \approx 2ST_R^2 \tag{30}$$

where we have assumed $\Delta T \ll T_R$. Equations 29 and 30 impose a constraint for applied biases which allow the thermoelectric refrigeration. The nanorefrigerator functions only when $V_{el}^{th,lower} < V_B < V_{el}^{th,upper}$. Equation 29 shows that the lower threshold bias $V_{el}^{th,lower}$ slightly decreases as T_R and ΔT increase. Equation 30 predicts that the upper threshold bias $V_{el}^{th,upper}$ increases as T_R increases.

We note that J_{el}^{R} is a function of bias V_B, T_R, and ΔT. For a given bias V_B and a given temperature difference ΔT, J_{el}^{R} is a function of T_R. We observe that there is a lower limit of temperatures when the thermoelectric refrigerator is working. The onset temperature for refrigeration effect, denoted as T_{el}^{OP}, is defined by $J_{el}^{R}(T_{el}^{OP}) = 0$. The nanorefrigerator is not functioning $(J_{el}^{R}(T_R) < 0)$ when $T_R < T_{el}^{OP}$. Especially, $J_{el}^{R}(T_R)$ can be expressed as a polynomial of T_R, derived from eq 26. If the Seebeck coefficient is sufficiently large and we neglect the terms higher than $O(T_R^2)$, the threshold operation temperature T_{el}^{OP} can be calculated analytically by solving the polynomial $J_{el}^{R}(T_R) = 0$, which gives

$$T_{el}^{OP} \approx \frac{1}{2}\left[\alpha/V_B + \sqrt{(\alpha/V_B)^2 + \beta V_B}\right] \tag{31}$$

where $\alpha = (\tau(\mu)\Delta T)/(\tau'(\mu)e)$ and $\beta = (6e\tau(\mu))/(\pi^2 k_B^2 \tau'(\mu))$. Equation 31 shows that T_{el}^{OP} increases as ΔT and V_B increase, respectively. When $\Delta T = 0$, $\alpha = 0$ and eq 31 approaches to

$$(T_{el}^{OP})_{min} \approx \sqrt{\frac{V_B T_R}{-2S}} \tag{32}$$

Equation 32 shows that T_{el}^{OP} approaches to the lower limit $(T_{el}^{OP})_{min}$ as $\Delta T \to 0$, where $(T_{el}^{OP})_{min}$ increases as $V_B \times T_R$ increases.

We now turn to investigating the COP of the thermoelectric cooling device. When V_B is small, $J_{el}^{L} - J_{el}^{R} = IV_B \approx \sigma V_B^2$. In this case, the COP is in the following form

$$\eta_{el} \approx \frac{J_{el}^{R}}{\sigma V_B^2} \tag{33}$$

where $J_{el}^{R}(V_B)$ is a polynomial of V_B given by eq 25. The applied biases considered in this study are small, hence we can consider $J_{el}^{R}(V_B)$ [given by eq 27] up to $O(V_B)$. Thus, eq 33 takes the form

$$\eta_{el} \approx \frac{-a + bV_B}{\sigma V_B^2} \tag{34}$$

The maximum value of COP (denoted as η_{max}^{el}) occurs at $\eta'(V_{max}^{\eta}) = 0$, which gives

$$\eta_{max}^{el} \approx \frac{3e^2 S^2 T_R}{4\pi^2 k_B^2 \Delta T} - \frac{1}{2} \tag{35}$$

where the maximum value of η_{el} occurs at bias $V_B = V_{max}^{\eta el}$, where

$$V_{max}^{\eta_{el}} \approx 2V_{el}^{th,lower} \tag{36}$$

where $V_{el}^{th,lower}$ is given by eq 29.

II. C. 2. Effect of the Phonon's Thermal Current. The phonon's thermal current flows from the hot to cold reservoir. It is an adverse effect to thermoelectric refrigeration because it heats up cold electrodes. To realize the impact of this adverse effect on refrigeration, we consider the weak-link model suitable for describing the heat transport for two thermal reservoirs connected by a weak elastic link.[68] In the low-temperature regime ($T \ll T_D$, where $T_D = 394$ K is the Debye temperature for Al), eq 21 can be expanded up to the lowest order in temperatures

$$J_{ph}^{R} = \lambda(T_R^4 - T_L^4) \tag{37}$$

where $\lambda \approx 2\pi^5 K^2 C^2 k_B^4/(15\hbar)$, where K is the stiffness of the nanostructured object bridging the metal electrodes, and C is the slope of the surface phonon's dispersion function in the long wavelength limit. The effect of the phonon's thermal current on refrigeration is described by a single parameter λ, which is determined by K and C. The simplified weak link model allows us to develop an analytical theory to investigate the effect of the phonon's thermal current on refrigeration using a single parameter λ. The influence of the strength of the phonon's thermal current on thermoelectric refrigeration becomes transparent.

To determine the impact of the phonon's thermal current (J_{ph}^{R}), we repeat similar discussions in the previous subsection for the thermoelectric nanorefrigerators. Correspondingly, the COP

of the thermoelectric nanorefrigerator becomes

$$\eta^{\mathrm{el+ph}} = \frac{J^{\mathrm{R}}_{\mathrm{el+ph}}}{IV_{\mathrm{B}}} \tag{38}$$

where $J^{\mathrm{R}}_{\mathrm{el+ph}} = J^{\mathrm{R}}_{\mathrm{el}} + J^{\mathrm{R}}_{\mathrm{ph}}$ is the combined thermal current including the phonon's thermal current.

We assume that $\Delta T \ll T_{\mathrm{R}}$, and eq 37 is approximated as

$$J^{\mathrm{R}}_{\mathrm{ph}} \approx -4\lambda T^3_{\mathrm{R}}\Delta T \tag{39}$$

Using eqs 27 and 39, the combined thermal current can be expressed in terms of a polynomial of V_{B} similar to eq 27

$$J^{\mathrm{R}}_{\mathrm{el+ph}} = -a_{\mathrm{el+ph}} + bV_{\mathrm{B}} - cV^2_{\mathrm{B}} - dV^3_{\mathrm{B}} \tag{40}$$

where $a_{\mathrm{el+ph}} = 2\pi^2 k^2_{\mathrm{B}}\tau(\mu)T_{\mathrm{R}}\Delta T/(3h) + 4\lambda T^3_{\mathrm{R}}\Delta T$, and the coefficients b, c, and d remain the same as those in eq 27.

An analogy can be drawn here between eqs 40 and 27 and likewise between eqs 38 and 25. Consequently, the equations in the previous section can be easily replicated here. In the presence of the phonon's thermal current, the working condition of the nanorefrigerator becomes

$$-S > \sqrt{\left(\frac{2\pi^2 k^2_{\mathrm{B}}}{3e^2} + \lambda\frac{8T^2_{\mathrm{R}}}{\sigma}\right)\left(\frac{\Delta T}{T_{\mathrm{R}}}\right)} \tag{41}$$

where λ represents the strength of the phonon's thermal current, and σ is the electric conductance of the nanojunction. As the phonon's thermal current vanishes ($\lambda = 0$), eq 41 restores eq 28. A sufficiently large phonon's thermal current has a large value of λ, which is likely to break down the inequality described in eq 41 and ruin refrigeration capability. Equation 41 shows that the phonon's thermal current is an adverse effect to thermoelectric refrigeration.

Similar to Section II. C, the thermoelectric nanorefrigeration works in a small range of biases. For a given T_{R} and a given temperature difference ΔT, $J^{\mathrm{R}}_{\mathrm{el+ph}}(V_{\mathrm{B}})$ is a function of bias V_{B}. We note that $J^{\mathrm{R}}_{\mathrm{el+ph}}$ is negative at $V_{\mathrm{B}} = 0$; therefore, a minimum bias (denoted as $V^{\mathrm{th,lower}}_{\mathrm{el+ph}}$) is needed to trigger a possible thermoelectric cooling effect. Similarly, the upper threshold bias $V^{\mathrm{th,upper}}_{\mathrm{el+ph}}$ is defined as the second zero of $J^{\mathrm{R}}_{\mathrm{el}}(V_{\mathrm{B}}) = 0$. Owing to $\Delta T \ll T_{\mathrm{R}}$ and the small values of $V^{\mathrm{th,lower}}_{\mathrm{el+ph}}$ and $V^{\mathrm{th,upper}}_{\mathrm{el+ph}}$, the lower threshold bias becomes

$$V^{\mathrm{th,\,lower}}_{\mathrm{el+ph}} \approx V^{\mathrm{th,\,lower}}_{\mathrm{el}} + \lambda[4T^2_{\mathrm{R}}\Delta T/(-S)\sigma] \tag{42}$$

where $V^{\mathrm{th,lower}}_{\mathrm{el}}$ is given by eq 29 which is analogous to eq 42. The lower threshold bias $V^{\mathrm{th,lower}}_{\mathrm{el+ph}}$ increases as the intensity of the phonon's thermal current (λ) increases. Similarly, the upper threshold bias $V^{\mathrm{th,upper}}_{\mathrm{el+ph}}$ is given by

$$V^{\mathrm{th,\,upper}}_{\mathrm{el+ph}} \approx V^{\mathrm{th,\,upper}}_{\mathrm{el}} - \lambda[4T^2_{\mathrm{R}}\Delta T/(-S)\sigma] \tag{43}$$

where $V^{\mathrm{th,upper}}_{\mathrm{el}}$ is given by eq 30. The upper threshold bias $V^{\mathrm{th,upper}}_{\mathrm{el+ph}}$ decreases as the intensity of the phonon's thermal current (λ) increases. The range of working biases shrinks by the phonon's thermal current, as given by eqs 43 and 43.

For a fixed ΔT, the functioning of the thermoelectric refrigerator is restricted to a range of temperatures between $T^{\mathrm{OP}}_{\mathrm{low}}$ and $T^{\mathrm{OP}}_{\mathrm{high}}$ obtained from eq 41. The lower and upper bounds of the operation temperatures are given by

$$T^{\mathrm{OP}}_{\mathrm{low,\,el+ph}} = \frac{S^2 + \sqrt{S^2 - \lambda\left(\frac{64\pi^2 k^2_{\mathrm{B}}\Delta T}{3e\sigma}\right)}}{\lambda(16\Delta T/\sigma)} \tag{44}$$

and

$$T^{\mathrm{OP}}_{\mathrm{high,\,el+ph}} = \frac{S^2 - \sqrt{S^2 - \lambda\left(\frac{64\pi^2 k^2_{\mathrm{B}}\Delta T}{3e\sigma}\right)}}{\lambda(16\Delta T/\sigma)} \tag{45}$$

Finally, we investigate the maximum value of the COP for a fixed T_{R} and a fixed temperature difference ΔT. The optimized COP considering the phonon's thermal current is given by

$$\eta^{\mathrm{max}}_{\mathrm{el+ph}} \approx \left[(\eta^{\mathrm{max}}_{\mathrm{el}})^{-1} + \lambda\left(\frac{16T_{\mathrm{R}}\Delta T}{S^2\sigma}\right)\right]^{-1} \tag{46}$$

where $\eta^{\mathrm{max}}_{\mathrm{el}}$ is the upper limit of COP given by eq 35 which is analogous to eq 46.

II. C. 3. Effect of Local Heating. Following the work of Chen, Zwolak, and Di Ventra,[22] the many-body Hamiltonian of the system, which considers the vibration of the atom/molecule bridging the electrodes, is

$$H = H_{\mathrm{el}} + H_{\mathrm{vib}} + H_{\mathrm{el-vib}} \tag{47}$$

where H_{el} is the electronic part of the Hamiltonian under adiabatic approximations and H_{vib} is the ionic part of the Hamiltonian considered in normal coordinates

$$H_{\mathrm{vib}} = \frac{1}{2}\sum_{j\in\mathrm{vib}}\dot{q}^2_j + \frac{1}{2}\sum_{j\in\mathrm{vib}}\omega^2_j q^2_j \tag{48}$$

where $\{\omega_j\}_{j=1,3N}$ are the normal-mode frequencies; $\{q_j\}_{j=1,3N}$ are the normal coordinates which are related to the Cartesian coordinates by

$$(\mathbf{Q}_i)_\mu = \sum_{j\,\in\,\mathrm{vib}} A_{i\mu,j}q_j \tag{49}$$

where $\mathbf{Q}_i = \mathbf{R}_i - \mathbf{R}^0_i$ is a small deviation of the ith ion from its equilibrium position $\mathbf{R}^0_i$ and μ {$= x, y, z$} denotes the {x, y, z}-component; $A_{i\mu,j}$ is a transformation between normal and Cartesian coordinates satisfying the canonical transformation: $\Sigma_{i,\mu}A_{i\mu,j}A_{i\mu,j'} = \delta_{j,j'}$. $H_{\mathrm{el-vib}}$ is a part of the Hamiltonian for electron−vibration interactions which has the form of

$$H_{\mathrm{el-vib}} = \sum_{\alpha,\beta,E_1,E_2,j}\left(\sum_{i,\mu}\sqrt{\frac{\hbar}{2M_i\omega_j}}A_{i\mu,j}J^{i\mu,\alpha\beta}_{E_1,E_2}\right) \cdot a^{\alpha\dagger}_{E_1}a^{\beta}_{E_2}(b_j + b^{\dagger}_j) \tag{50}$$

where $\alpha,\beta = \{L,R\}$; M_i is the mass of the ith atom; $b_j(b^{\dagger}_j)$ are the phonon annihilation (creation) operators for the jth vibrational mode of nanoscale junctions which satisfy the commutation relation $[b_j, b^{\dagger}_{j'}] = \delta_{j,j'}$; and $\{a^{\mathrm{L(R)}}_E\dagger, a^{\mathrm{L(R)}}_E\}$ are the creation and annihilation operators, respectively, for incident electrons with energy E from the left (right) electrode. They satisfy the usual anticommutation relation, $\{a^{\alpha}_{E1}, a^{\beta\,\dagger}_{E2}\} = \delta_{\alpha\beta}\delta(E_1 - E_2)$; the

dx.doi.org/10.1021/jp110920q |J. Phys. C 2011, 115, 6111–6125

coupling constant $J^{i\mu,\alpha\beta}_{E1,E2}$ between electrons and the vibration of the ith atom in the μ (=x, y, z) component can be calculated as

$$J^{i\mu,\alpha\beta}_{E_1,E_2} = \int d\mathbf{r} \int d\mathbf{K}_{\parallel} [\Psi^{\alpha}_{E_1\mathbf{K}_{\parallel}}(\mathbf{r})]^* [\partial_{\mu} V^{\mathrm{ps}}(\mathbf{r},\mathbf{R}_i) \Psi^{\beta}_{E_2\mathbf{K}_{\parallel}}(\mathbf{r})] \quad (51)$$

where $V^{\mathrm{ps}}(\mathbf{r},\mathbf{R}_i)$ is the pseudopotential representing the interaction between electrons and the ith ion, and $\Psi^{\alpha(=\mathrm{L,R})}_{E\mathbf{K}_{\parallel}}(\mathbf{r})$ stands for the effective single-particle wave function of the entire system corresponding to incident electrons propagated from the left (right) electrode. These wave functions are calculated iteratively until convergence and self-consistency are achieved in the framework of DFT combined with the Lippmann−Schwinger equation.[73]

We now use the first-order time-independent perturbation theory to approximate the wave function. The unperturbed system where electron−phonon scattering is absent can be described by $|\Psi^{\mathrm{L(R)}}_E;n_j\rangle = |\Psi^{\mathrm{L(R)}}_E\rangle \otimes |n_j\rangle$ where $|n_j\rangle$ is the phonon state of the jth normal mode.[23] In Figure 2, we display eight different electron−phonon scattering processes when electrons tunnel through nanoscale junctions.

Since electron−vibration interaction is directly related to junction heating, we also include local heating in our Seebeck coefficient calculations. Details of the theory of local heating in nanoscale structures can be found in ref 22. The power absorbed and emitted by electrons incident from the β = {L,R} electrode to the α = {L,R} electrode via a vibrational mode j is denoted by $W^{\alpha\beta,k}_j$. The total thermal power P generated in the junction can be written as the sum over all vibrational modes of eight scattering processes shown in Figure 2

$$P = \sum_{j \in \mathrm{vib}} (W^{\mathrm{RR},2}_j + W^{\mathrm{RL},2}_j + W^{\mathrm{LR},2}_j + W^{\mathrm{LL},2}_j - W^{\mathrm{RR},1}_j - W^{\mathrm{RL},1}_j - W^{\mathrm{LR},1}_j - W^{\mathrm{LL},1}_j) \quad (52)$$

where $W^{\alpha\beta,k}_j$ are calculated from the Fermi golden rule

$$W^{\alpha\beta,k}_j = 2\pi\hbar(\delta_{k,2} + \langle n_j\rangle) \int dE \left| \sum_{i,\mu} A_{i\mu,j} J^{i\mu,\alpha\beta}_{E \pm \hbar\omega_j, E} \right|^2 \cdot f_E(\mu_\alpha, T_\alpha)[1 - f_{E \pm \hbar\omega_j}(\mu_\beta, T_\beta)] D^{\alpha}_{E \pm \hbar\omega_j} D^{\beta}_{E} \quad (53)$$

where α,β ={L,R} and $\delta_{k,2}$ is the Kronecker delta and k = 1 (2) corresponding to relaxation (excitation) of the vibrational modes; D^{α} is partial density of states corresponding to Ψ^{α}_E; and the ensemble average of occupation number of the jth vibrational mode is $\langle n_j\rangle = 1/\{\exp[\hbar\omega_j/(k_B T_w)] - 1\}$, where T_w is the effective wire temperature. The majority of the heat generation in the central region of the atomic junction is transferred to electrodes. We estimate the rate of heat dissipation using the simplified weak link model. We assume that the rate of thermal current from the junction with temperature T_w dissipated to the left electrode with temperature T_L is equivalent to the thermal current of a weak thermal link between reservoirs with temperature T_L and $T_R = 2T_w - T_L$. The rate of heat generation transferred to the left electrode is, therefore, approximated to

$$J^{\mathrm{L}}_{\mathrm{localheating}} = \lambda(2T_w - T_L)^4 - T_L^4] \quad (54)$$

Similarly, the rate of heat generation transferred to the left electrode approximately is

$$J^{\mathrm{R}}_{\mathrm{localheating}} = \lambda[(2T_w - T_R)^4 - T_R^4] \quad (55)$$

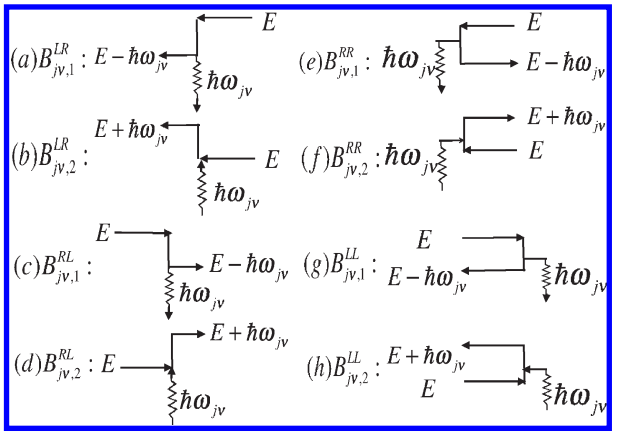

Figure 2. Feymann diagrams of the first-order electron−vibration scattering processes considered in this study.

The effective local temperature T_w is obtained when heat generation in the nanostructure [eq 52] and heat dissipation into the bulk electrodes [eqs 54 and 55] reach balance

$$P_{\mathrm{localheating}} = J^{\mathrm{L}}_{\mathrm{localheating}} + J^{\mathrm{R}}_{\mathrm{localheating}} \quad (56)$$

We calculate the effective local temperature T_w by solving eq 56. When considering the effect of local heating and the phonon's thermal current, the rate of the heat energy extracted from the cold (right) reservoir is

$$J^{\mathrm{R}}_{\mathrm{el+ph+heating}} = J^{\mathrm{R}}_{\mathrm{el+ph}} - J^{\mathrm{R}}_{\mathrm{localheating}} \quad (57)$$

and the corresponding COP of the thermoelectric nanorefrigerator becomes

$$\eta_{\mathrm{el+ph+heating}} = \frac{J^{\mathrm{R}}_{\mathrm{el+ph+heating}}}{IV_B} \quad (58)$$

III. RESULTS AND DISCUSSION

This study proposes a thermoelectric cooling device based on an atomic-sized junction. We developed an analytical theory and first-principles calculations for the electronic cooling including the effect of the phonon's thermal current and local heating. The theory is applied to investigate an ideal 4-Al monatomic chain sandwiched between two bulk Al electrodes. In Section III. A we discuss the enhanced Seebeck effect due to the P_x−P_y orbital near the chemical potential and the influence of the phonon's thermal current on ZT. A large Seebeck coefficient is of crucial importance for the design of thermoelectric nanodevices. Therefore, we investigate the thermoelectric properties of the 4-Al atomic junction as follows. In Sections III. B, III. C, and III. D, we discuss the thermoelectric cooling effect without and with the phonon's thermal current and local heating. The 4-Al thermoelectric junction serves as an example illustrating the advantage of nanoscale refrigerators, where the overwhelming Joule heat in the bulk system and photon radiation are strongly suppressed due to size reduction. These properties facilitate possible thermoelectric cooling in the 4-Al junction beyond the expectation of conventional solid-state device theory.

III. A. Thermoelectric Properties of the 4-Al Atomic Junction. We apply the theory and first-principles calculations shown in Section II to a 4-Al atomic junction as a thermoelectric cooling

dx.doi.org/10.1021/jp110920q |J. Phys. Chem. C 2011, 115, 6111–6125

device, as depicted in Figure 1(a). The 4-Al atomic junction is electronically simple such that the first-principle calculations reported here can be performed with a high level of accuracy. The aluminum junction is, therefore, an ideal testbed for comparing quantum transport theory under nonequilibrium and experiments.[66,67]

We begin our discussion by considering an ideal 4-Al atomic chain bridging two bulk Al metal electrodes that we model as ideal metals (jellium model, $r_s \approx 2$). The nanostructured object is considered as a scattering center. The scattered wave functions of the whole system are calculated by solving the Lippmann−Schwinger equation iteratively until self-consistency is obtained. We assume that the left and right electrodes are independent electron and phonon reservoirs ($T_R = T_C$; $T_L = T_R + \Delta T = T_H$), respectively, with the electron and phonon population described by the Fermi−Dirac and Bose−Einstein distribution function. Two electrodes are connected to a battery with an applied bias $V_B = (\mu_R - \mu_L)/e$, where μ_L and μ_R are the chemical potential deep in the left and right electrodes, respectively. A detailed account of the theory is given in Section II. A.

The Seebeck coefficients are calculated from first-principles using the transmission function obtained from the DFT calculations, as described in eq 9. The 4-Al atomic junction is marked by a sigma channel near the chemical potentials with the P_x-P_y orbital characters, as shown in Figure 1(b). The Seebeck coefficients correlate highly with the magnitudes and slopes of DOSs near the chemical potentials, as described in eq 11. The sigma channel leads to a large value in the slope of the transmission function near the chemical potentials. This gives rise to a larger Seebeck coefficient, as shown in Figure 1(c), which compares favorably with those of Pt, Pd, and Au atomic chains.

The efficiency of energy conversion in the thermoelectric junction is usually described by the figure of merit (denoted as ZT), as defined in eq 23. When ZT tends to infinity, the thermoelectric efficiency will reach the Carnot efficiency, the upper limit of energy conversion efficiency. ZT depends on the following physical factors: the Seebeck coefficient (S), the electric conductance (σ), the electron's thermal conductance (κ_{el}), and the phonon's thermal conductance (κ_{ph}). These physical factors can be evaluated using eqs 9, 18, 13, and 37, respectively. To obtain a large ZT value, the thermoelectric nanojunction will require a large value of S, a large value of σ, and a small value of the combined heat conductance ($\kappa = \kappa_{el} + \kappa_{ph}$). Thermoelectric devices with a large value of σ are usually accompanied by a large value of κ_{el}, due to the same proportionality with the transmission function. These values are highly correlated, making the enhancement of the thermoelectric figure of merit ZT a challenging task.

The thermal energy carried by phonons flows from the hot into the cold reservoir. The phonon's thermal current takes heat into the cold reservoir, and it, thus, is a negative effect on the thermoelectric refrigeration. We consider the phonon's thermal current in the weak link model [as described in eq 19], where each electrode is assumed to be in thermodynamic equilibrium, joined by a weak mechanical link modeled by a harmonic spring of stiffness K. In the weak-tunneling limit, the weak link model can be interpreted as an application of the thermal Landauer formula.[68] Up to the leading order in temperatures, we expand eq 19 which gives a simple form, $J_{ph}^R = \lambda(T_R^4 - T_L^4)$ [i.e., eq 37 specified as the simplified weak link model], where $\lambda \approx 2\pi^5 K^2 C^2 k_B^4/(15\hbar)$. Simplification allows us to investigate the effect of the phonon's thermal current with a single parameter λ, which is determined by the stiffness of the nanostructured object (K) and the slope of the electrodes's surface phonon's spectral density (C). The simplified weak link model is valid in the small temperature regime (TT_D, where T_D = 394 K is the Debye temperature for Al). We note that the simplified weak link model violates the Wiedemann−Franz law in the low-temperature regime, while eq 19 restores the Wiedemann−Franz law at TT_D. The range of temperatures discussed in this study mostly lies within the valid regime of the simplified weak link model. Therefore, we consider ZT as a function of temperatures in the presence of the phonon's thermal current of which is represented by various values of λ, as shown in Figure 1(d). The validity of the λ values for linear atomic wires will be justified later in Section III. C.

III. B. Thermoelectric Cooling Effect in the Absence of Phonon's Thermal Current and Local Heating. Let us now attempt to investigate the 4-Al junction as a thermoelectric cooling device from the first-principles approaches. For the present, we shall confine our attention to the simplest case, the one which neglects the phonon's thermal current and local heating. Effects of the phonon's thermal current and local heating will be discussed in Sections III. C and III. D. We also put forward an analytical theory to explain the numerical results. The analytical theory described below is general to any atomic/molecular thermoelectric junction as a thermoelectric nanorefrigerator.

When an external bias is applied, electrons flow from the right to the left electrodes. The flow of electrons carries not only the charge current but also the energy current. The thermal current carried by electrons [denoted as $J_{el}^{R(L)}(\mu_L,T_L;\mu_R,T_R)$], defined as the rate at which thermal energy flows from the right (into the left) electrode, can be calculated from first-principles using eq 7 with the help of the wave functions obtained self-consistently in the DFT calculations. Note that $J_{el}^R + IV_B = J_{el}^L$ [for details, see eq 24] because of energy conservation. It implies that the thermoelectric refrigeration requires electric power IV_B to remove thermal energy from the cold (right) reservoir (with rate J_{el}^R) and reject waste thermal energy to the hot (left) reservoir (with rate J_{el}^R). The nanorefrigerator works when $J_{el}^R > 0$. As noted in eq 7, J_{el}^R is a function of V_B, ΔT, and T_R. Note that $J_{el}^R(T_R = 0) < 0$. At a given V_B and ΔT, the smallest solution of $J_{el}^R(T_R) = 0$ defines the threshold operation temperature, denoted as T_{el}^{OP}, below which the nanorefrigerator does not function. Figure 3(a) shows the T_{el}^{OP} of the 4-Al nanorefrigerator as a function of ΔT and V_B. The operating temperature of the 4-Al nanorefrigerator can be lower than 100 K, as shown in Figure 3(a).

To enrich the understanding of thermoelectric nanorefrigerators, we also propose an analytical theory that provides guidelines for the design of nanorefrigerators. When $\Delta T \ll T_R$, the application of the Sommerfeld expansion on eq 7 can simplify the electron's thermal current J_{el}^R as a polynomial of V_B, as described in eq 27. If the higher-order term V_B^3 is neglected, the maximum of $J_{el}^R(T_R)$ that is greater than zero yields a criterion for the existence of thermoelectric cooling, which gives eq 28: $-S > \pi k_B[2\Delta T/(3T_C)]^{1/2}/e$, where T_C (=T_R) is the temperature of the cold (right) reservoir, $S = -\pi^2 k_B^2 \tau'(\mu) T_R/[3e\tau(\mu)]$ is the Seebeck coefficient, k_B is the Boltzmann constant, and e is the electron charge. To have a possible refrigeration effect, the Seebeck coefficient S, the temperature difference ΔT, and the temperature of the cold reservoir T_C need to satisfy eq 28. The choice of an n-type thermoelectric junction with a large Seebeck coefficient is of crucial importance in the design of thermoelectric

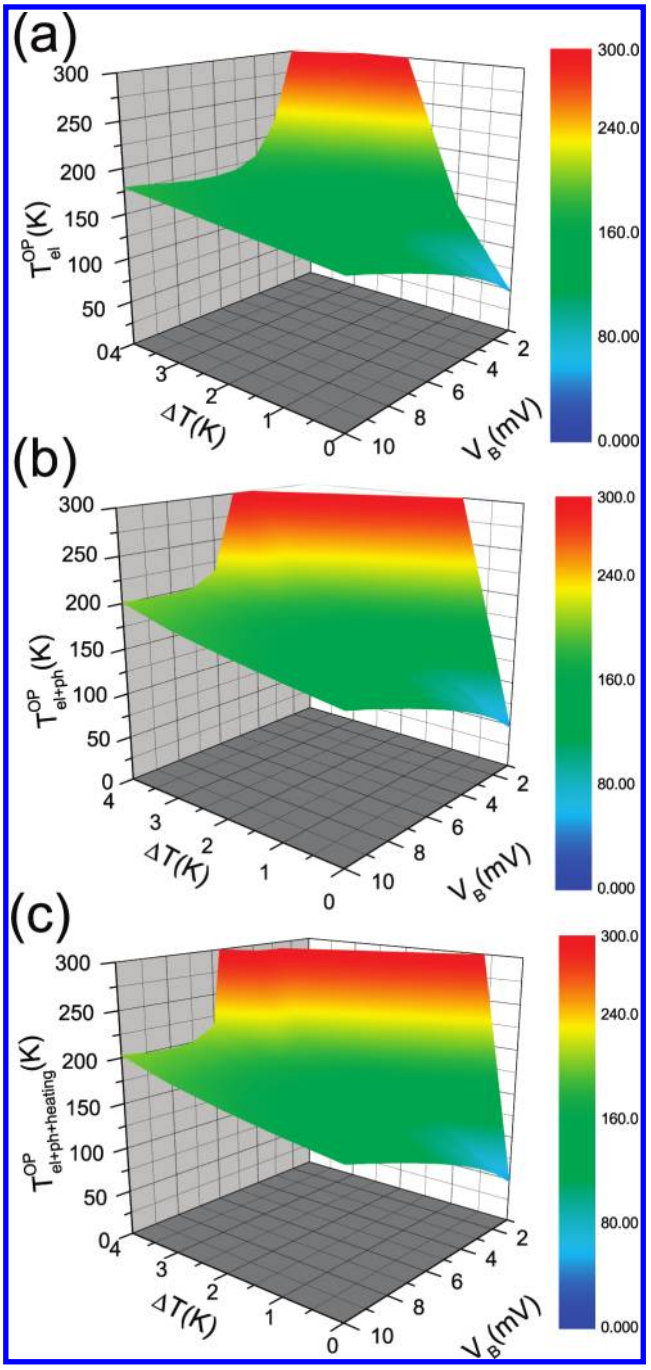

Figure 3. (a) Critical operation temperature T_{el}^{OP} vs ΔT and V_B in the absence of the phonon's thermal current. (b) T_{el+ph}^{OP} vs ΔT and V_B in the presence of the phonon's thermal current with $\lambda = 10^{-17}$ W/K^4. (c) $T_{el+ph+heating}^{OP}$ vs ΔT and V_B in the presence of local heating and the phonon's thermal current with $\lambda = 10^{-17}$ W/K^4.

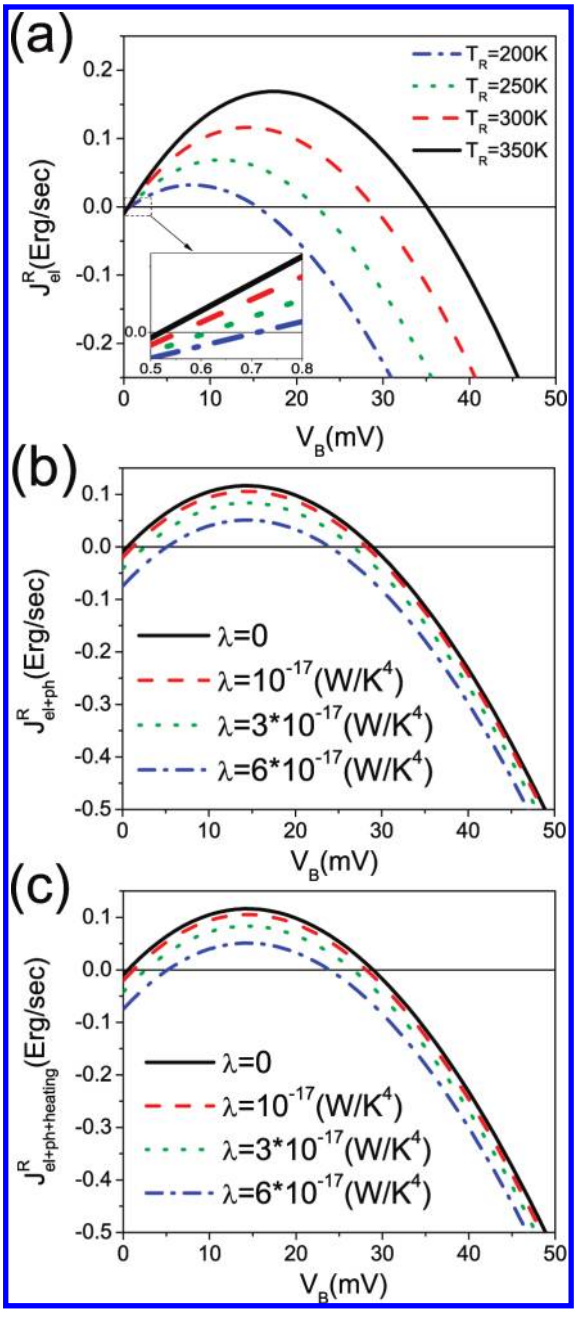

Figure 4. (a) J_{el}^R vs V_B for various values of T_R in the absence of the phonon's thermal current, where $\Delta T = 1$ K. (b) J_{el+ph}^R vs V_B for $\lambda = 0$, 1×10^{-17}, 3×10^{-17}, and 6×10^{-17} W/K^4 in the presence of the phonon's thermal current, where $\Delta T = 1$ K and $T_R = 300$ K. (c) $J_{el+ph+heating}^R$ vs V_B for $\lambda = 0$, 1×10^{-17}, 3×10^{-17}, and 6×10^{-17} W/K^4 in the presence of local heating and the phonon's thermal current, where $\Delta T = 1$ K and $T_R = 300$ K.

nanorefrigerators. Large Seebeck coefficients could be achieved through an appropriate choice of bridging nanostructured objects and further optimized by applying gate voltages.[40,50]

Figure 4(a) shows the rate of thermal energy extracted from the cold temperature reservoir (J_{el}^R) as a function of V_B for T_R = 200, 250, 300, and 350 K, where the temperature difference between the hot and cold reservoir ΔT is fixed at 1 K. We note that $J_{el}^R < 0$ at zero bias [see Figure 4(a)], and thus a lower threshold voltage $V_{el}^{th,lower}$ for the battery, is needed to trigger the refrigeration effect. The lower threshold bias is defined as the smallest positive solution of $J_{el}^R(V_B) = 0$ for a given T_R and ΔT. When $V_B < V_{el}^{th,lower}$, the rate of thermal energy removed from the cold reservoir is negative ($J_{el}^R < 0$), and thus the thermoelectric nanorefrigerator does not function. We also observe an upper threshold voltage $V_{el}^{th,upper}$ for the refrigeration effect. When $V_B > V_{el}^{th,upper}$, the rate of thermal energy removed from the cold reservoir is also negative ($J_{el}^R < 0$), and thus the thermoelectric nanorefrigerator loses the capability of refrigeration.

dx.doi.org/10.1021/jp110920q |J. Phys. Chem. C 2011, 115, 6111–6125

Since $V_{el}^{th,lower}$ and $V_{el}^{th,upper}$ have very small values, we neglect the terms higher than the second order of V_B in eq 27 and obtain $V_{el}^{th,lower}$ and $V_{el}^{th,upper}$ from $J_{el}^{R}(V_B) = 0$, as described in eqs 29 and 30, where we assumed $\Delta T \ll T_R$. Equation 29 predicts that the lower threshold voltage, $V_{el}^{th,lower} \approx -\pi^2 k_B^2 \Delta T/(3e^2 S T_R)$, decreases as T_R increases, as shown in the inset of Figure 4(a). Equation 30 predicts that the upper threshold voltage, $V_{th,upper}^{el} \approx 2ST_R^2$, increases as T_R increases. Concluding from eqs 29, 30, and 35, the refrigeration effect is triggered at around $V_B = V_{el}^{th,lower}$, optimized around $V_B = 2V_{el}^{th,lower}$, and loses the refrigeration capability at $V_B = V_{el}^{th,upper}$.

Figure 5(a) shows J_{el}^{R} as a function of T_R for different values of $\Delta T = 0$, 1, 2, 3, and 4 K, where the bias is fixed at $V_B = 6$ mV. For a given V_B and ΔT, we define the critical operation temperature T_{el}^{OP} as the solution of $J_{el}^{R}(T_R) = 0$. The thermoelectric nanorefrigerator is working when $T_R > T_{el}^{OP}$. The critical operation temperature can be calculated from eq 26: $T_{el}^{OP} \approx (1/2)[(\alpha - 1)\Delta T + ((\alpha^2 - 1)\Delta T^2 + \beta)^{1/2}]$, where $\alpha = \tau(\mu_L)/[\tau'(\mu_L)eV_B]$ and $\beta = -2V_B/S$. The foregoing equation predicts that T_{el}^{OP} increases as ΔT increases, which agrees well with the numerical calculation presented in Figure 5(a). If $\Delta T = 0$ K, then T_{el}^{OP} reaches the minimum value $(T_{el}^{OP})_{min} \approx [(T_R V_B)/(-2S)]^{1/2}$ as described in eq 32. The equation shows that $(T_{el}^{OP})_{min}$ increases as V_B increases and as T_R increases, respectively. At $V_B = 6$ mV, the $(T_{el}^{OP})_{min}$ for the 4-Al thermoelectric refrigerator is 116 K, which can be further suppressed by decreasing the bias V_B. Turning to the efficiency of the thermoelectric nanorefrigerator, the COP (denoted as η^{el}) is defined as the ratio of the rate of heat removed from the cold reservoir to the electric power supplied by the battery, that is, $\eta_{el} = J_{el}^{R}/(IV_B)$, as equivalent to eq 33. Derived from eq 34, the maximum value of COP is given by eq 35.

Figure 6(a) shows the numeric calculations of η_{el} as a function of V_B for $T_R = 200$, 250, 300, and 350 K, where $\Delta T = 1$ K. This figure also shows that the optimized COP (η_{el}^{max}) increases as T_R increases. The optimized COP occurs at bias $V_{max}^{\eta el} \approx 2V_{el}^{th,lower}$, where $V_{el}^{th,lower}$ is the lower threshold bias for possible refrigeration, as shown in Figure 7(a). We should note that the maximum value of COP can be greatly magnified by a suitable nanojunction with a large Seebeck coefficient according to $\eta_{el}^{max} \propto S^2$ as predicted in eq 35.

Figure 7(a) shows the numeric calculations of η_{el} as a function of V_B for $\Delta T = 1$, 2, 3, and 4 K, where $T_R = 200$ K. The exchange of energy by heat currents between the hot and cold reservoirs is an irreversible process and leads the decrease of the optimized COP as ΔT increases as described by eq 35: $\eta_{el}^{max} = 3e^2S^2T_R/(4\pi^2k_B^2\Delta T) - 1/2$. As a direct consequence of the above equation, the maximum value of COP (η_{el}^{max}) increases as T_R increases and as ΔT decreases. This prediction agrees well with eq 35.

III. C. Thermoelectric Cooling Effect Including the Phonon's Thermal Current. The phonon's thermal current carries thermal energy from the hot to cold reservoir, which is an adverse effect to refrigeration. To assess the extent of this adverse effect, we consider the phonon's thermal current within the simplified weak link model. The simplified weak link model is suitable for describing the heat transport for two thermal reservoirs connected by a weak elastic link in a low-temperature regime ($T \ll T_D$, where $T_D = 394$ K is the Debye temperature for Al) and is convenient to describe the phonon's thermal current by a single parameter λ: $J_{ph}^{R} = \lambda(T_R^4 - T_L^4)$, where $\lambda \approx 2\pi^5K^2C^2k_B^4/(15\hbar)$. The parameter λ can be determined by K and C, where K is the stiffness of the nanostructured object connecting to electrodes and C is the slope of the spectral density $N(E) \approx C \times E$. The simplified weak link model allows the construction of an analytical theory that offers a concise explanation for how the phonon's thermal current (represented by a single parameter λ) affects thermoelectric cooling.

From recent experiments,[70] it is observed that the stiffness of the linear Pt atomic chains varies in a wide range of several orders of magnitudes. This experiment suggests that the stiffness ($K \approx 0-1.2$ N/m) is likely to depend strongly on the detailed atomic

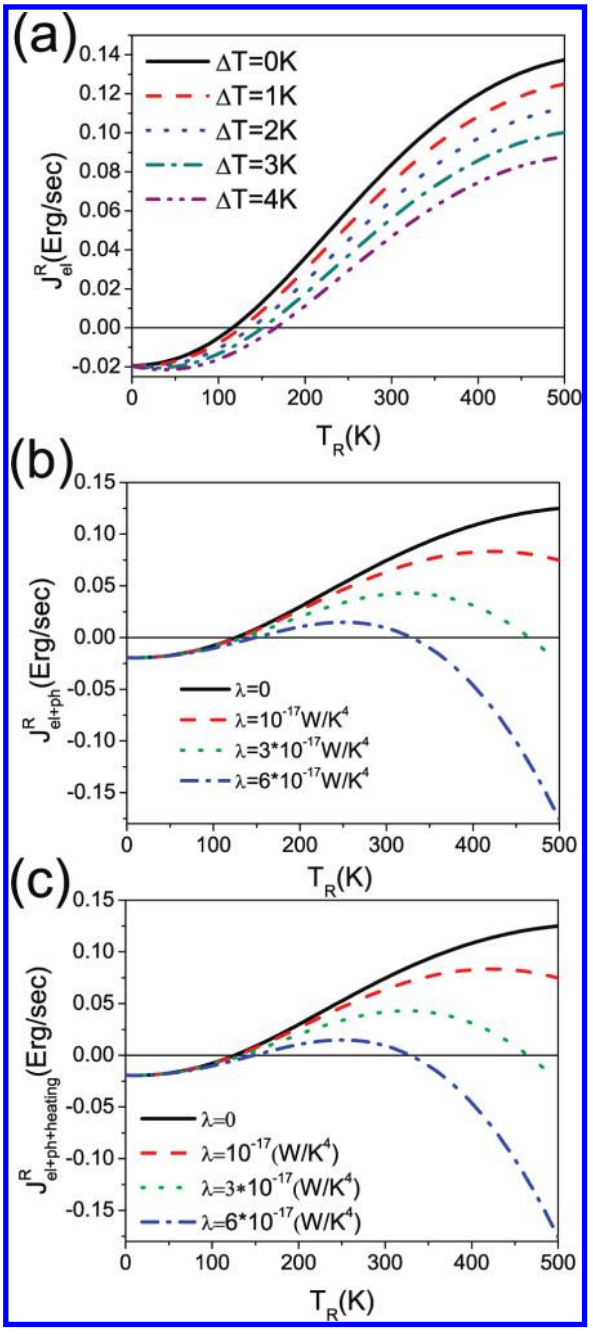

Figure 5. (a) J_{el}^{R} vs T_R for various values of $\Delta T = 0$, 1, 2, 3, and 4 K in the absence of the phonon's thermal current, where $V_B = 6$ mV. (b) J_{el+ph}^{R} vs T_R for $\lambda = 0$, 1×10^{-17}, 3×10^{-17}, and 6×10^{-17} W/K^4 in the presence of the phonon's thermal current, where $V_B = 6$ mV. (c) $J_{el+ph+heating}^{R}$ vs T_R for $\lambda = 0$, 1×10^{-17}, 3×10^{-17}, and 6×10^{-17} W/K^4 in the presence of local heating and the phonon's thermal current, where $V_B = 6$ mV.

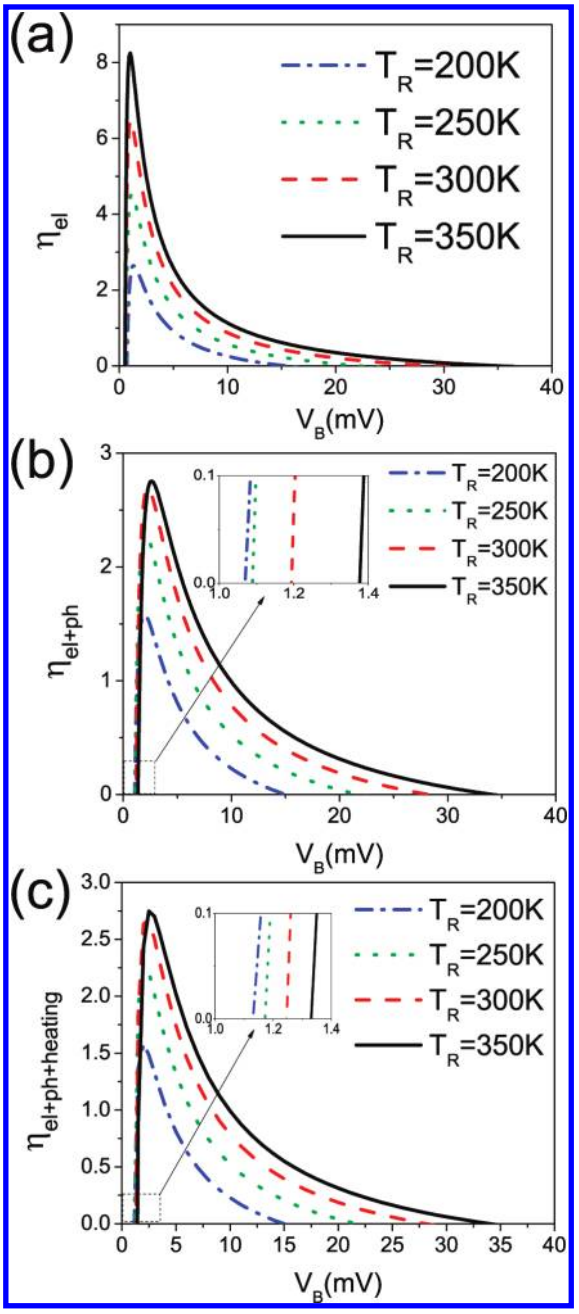

Figure 6. (a) COP (η_{el}) vs V_B in the absence of the phonon's thermal current for T_R = 200, 250, 300, and 350 K, where ΔT = 1 K. (b) η_{el+ph} vs V_B in the presence of the phonon's thermal current for T_R = 200, 250, 300, and 350 K, where ΔT = 1 K. (c) $\eta_{el+ph+heating}$ vs V_B in the presence of local heating and the phonon's thermal current for T_R = 200, 250, 300, and 350 K, where ΔT = 1 K.

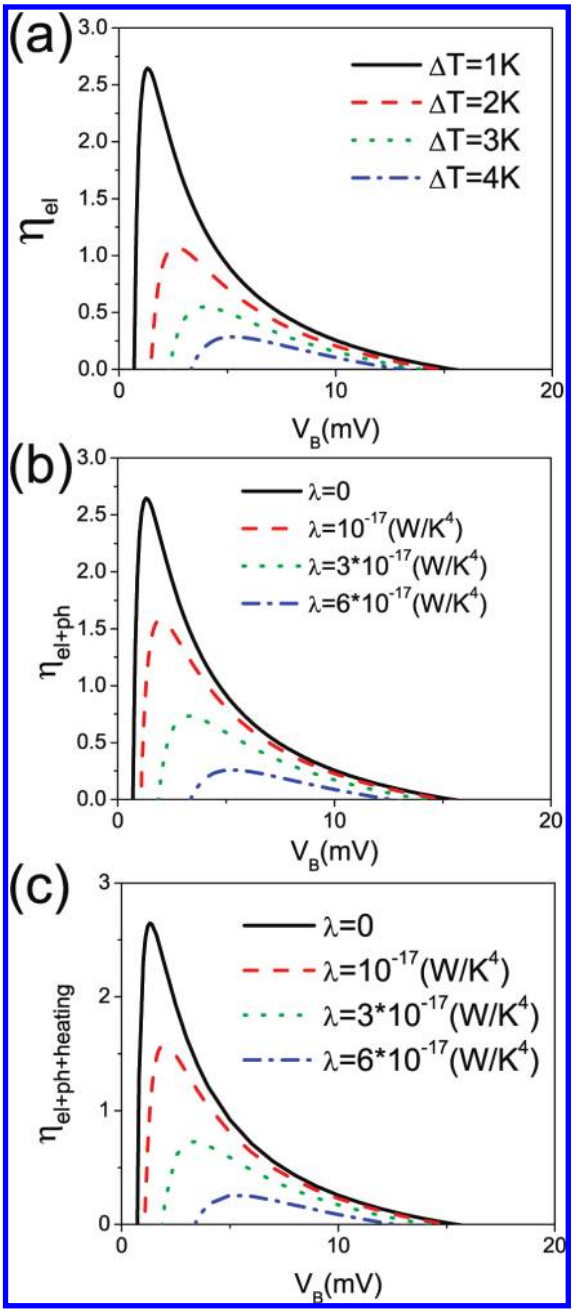

Figure 7. (a) η_{el} vs V_B in the absence of the phonon's thermal current for T_R = 200 K. (b) η_{el+ph} vs V_B in the presence of the phonon's thermal current for λ = 0, 1 × 10^{-17}, 3 × 10^{-17}, and 6 × 10^{-17} W/K^4, where ΔT = 1 K and T_R = 200 K. (c) $\eta_{el+ph+heating}$ vs V_B in the presence of local heating and the phonon's thermal current for λ = 0, 1 × 10^{-17}, 3 × 10^{-17}, and 6 × 10^{-17} W/K^4, where ΔT = 1 K and T_R = 200 K.

structure of the full system, especially in the contact region. For example, the monatomic chain could be particularly stiff along the chain direction when the atomic chain forms a perfectly straight line; otherwise, the atomic (zigzag) chain could easily bend with much smaller stiffness. In this view, the magnitudes of the phonon's thermal current could possibly vary in a wide range in nanojunctions formed by monatomic chains. This feature could allow the possibility (for example, zigzag chain instead of perfect linear chain) to suppress the phonon's thermal current by creating a suppression in the mechanic link. An estimation from the experimental data of K = 0−1.2 N/m and $C \approx 1.887 \times 10^8$ cm^2/erg^2 in the Pt atomic junction yields the values of λ in the range from 0 to 2.05 × 10^{-19} W/K^4.[70,71]

In the 4-Al atomic junction, we choose λ around the order of 10^{-17} W/K^4 to present the strength of the phonon's thermal current. In this range of λ, the effect of the phonon's thermal current on the thermoelectric refrigeration is salient. For the 4-Al monatomic junction, $\lambda \approx 5.7 \times 10^{-15}$ W/K^4, which is given by $K \approx 90.91$ N/m obtained from total energy calculations and $C \approx 7.62 \times 10^8$ cm^2/erg^2 from the surface phonon dispersion relation

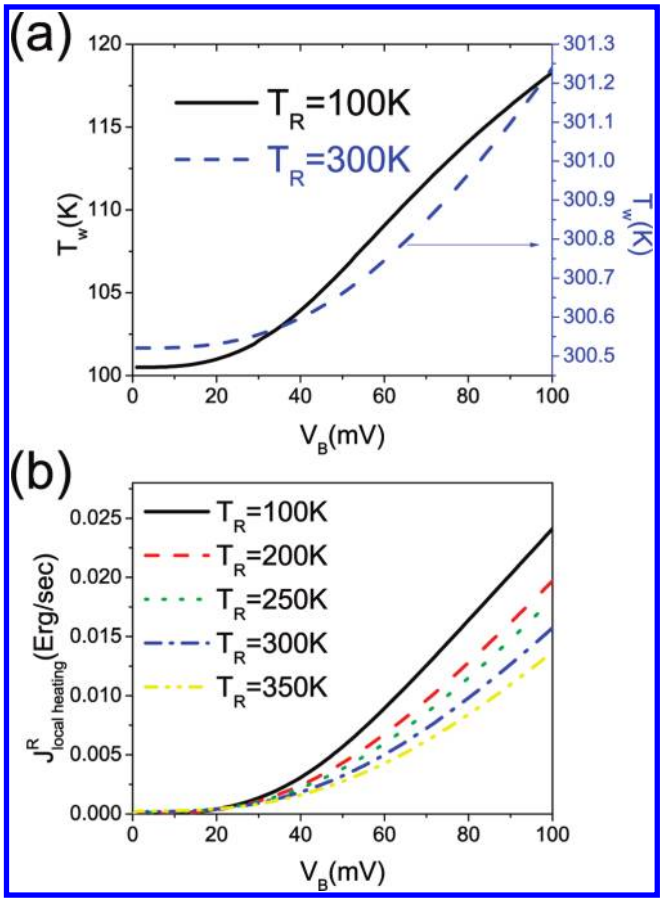

Figure 8. (a) Effective wire temperature T_w vs V_B for T_R = 100 K (left axis) and T_R = 300 K (right axis), where $\lambda = 1 \times 10^{-17}$ W/K^4. (b) The rate of heating energy dissipated to the cold reservoir $J^R_{\text{local heating}}$ vs V_B for T_R = 100, 200, 250, 300, and 350 K.

obtained from first-principle calculations.[72] However, this value is notably larger than the Pt monatomic chains with λ ranging from 0 to 2.05×10^{-19} W/K^4. The reason for this is that the stiffness of a 4-Al linear atomic chain is K = 90.91 N/m, which is notably larger than the stiffness of the Pt chain (K = 0−1.2 N/m) measured in the experiments. This experiment for a Pt monatomic chain infers that the stiffness K for the 4-Al junction could be overestimated by the total energy calculations, where the chain is assumed to be perfectly linear. In this viewpoint, the λ (around 10^{-17} W/K^4) we choose to present the strength of the phonon's thermal current for the 4-Al atomic junction could be reasonable.

In the presence of the phonon's thermal current, the COP is defined as $\eta_{el+ph} = (J^R_{el+ph})/(IV_B)$, where $J^R_{el+ph} = J^R_{el} + J^R_{ph}$ is the combined thermal current. In the presence of the phonon's thermal current, the functioning of the 4-Al atomic refrigerator requires higher operation temperatures (denoted as T^{OP}_{el+ph}), as shown in Figure 3(b), where we plot the operation temperature T^{OP}_{el+ph} as a function of V_B and ΔT with the strength of the phonon's thermal current described by the simplified weak link model with $\lambda = 10^{-17}$ W/K^4. Applying the Sommerfeld expansion, the combined thermal current J^R_{el+ph} can be expressed as a polynomial of V_B when $\Delta T \ll T_R$, as shown in eq 40. When the term V_B^3 is neglected in eq 40, the criterion for the existence of electronic cooling is given by eq 41: $-S > [(2\pi^2 k_B^2/(3e^2) + 8\lambda/\sigma)(\Delta T/T_R)]^{1/2}$. The criterion for possible thermoelectric refrigeration provides the guideline for devising experiments to test the effect of thermoelectric cooling at the atomic level. When $\lambda \to 0$, eq 41 restores eq 28 in the absence of the phonon's thermal current.

Figure 4(b) shows the combined thermal current J^R_{el+ph} as a function of V_B for $\lambda = 0, 1 \times 10^{-17}, 3 \times 10^{-17}$, and 6×10^{-17} W/K^4, where we fix ΔT = 1 K and T_R = 300 K. Note that $J^R_{el+ph} < 0$ at zero bias. Similar to the previous discussions in the absence of the phonon's thermal current, the thermoelectric nanorefrigerator works when $J^R_{el+ph} > 0$. This leads to the lower and upper bounds of threshold voltage, as given in eqs 42 and 43. The working bias which allows the operation of the thermoelectric nanorefrigerator is restricted to a small range of biases: $V^{th,lower}_{el+ph} < V_B < V^{th,upper}_{el+ph}$. Equations 42 and 43 show that the lower (upper) threshold bias $V^{th,lower}_{el+ph}$ ($V^{th,upper}_{el+ph}$) increases (decreases) by a value of $\lambda[4T_R^2\Delta T/(-S)\sigma]$ as the intensity of the phonon's thermal current (λ) increases. This leads to suppression of the range of working biases by the phonon's thermal current, which agrees well with the numerical calculations as shown in Figure 4(b).

Figure 5(b) shows the combined thermal current J^R_{el+ph} as a function of T_R for $\lambda = 0, 1 \times 10^{-17}, 3 \times 10^{-17}$, and 6×10^{-17} W/K^4, where we fix V_B = 6 mV and ΔT = 1 K. Figure 5(b) exhibits the combined thermal current J^R_{el+ph}, which could become negative at high-temperature regimes. The reason for this is that the phonon's thermal current brings heat from the hot to the cold reservoir. Thus, the combined thermal current becomes a negative value, which disables refrigeration capability at high temperatures. This imposes an upper limit for the working temperature, above which J^R_{el+ph} turns to be negative, and consequently the nanorefrigerator does not function. The operation of the nanorefrigerator is limited to a range of temperatures between $T^{OP}_{low,el+ph}$ and $T^{OP}_{high,el+ph}$, as described in eqs 44 and 45. As λ increases, eqs 44 and 45 predict that the range of operation temperatures shrinks, which agrees well with the numerical calculations as shown in Figure 5(b).

Figure 6(b) shows the numeric calculations of η_{el+ph} as a function of V_B for T_R = 200, 250, 300, and 350 K, where ΔT = 1 K is fixed. Equation 46 shows that the upper limit of COP (denoted as η^{max}_{el+ph}) is given by: $\eta^{max}_{el+ph} = [(\eta^{max}_{el})^{-1} + \lambda(16T_R\Delta T/(S^2\sigma))]^{-1}$. It shows that the upper limit of COP (η^{el+ph}_{max}) increases as λ increases as predicted by eq 46; meanwhile, the inset of Figure 6(b) shows that the $V^{th,lower}_{el+ph}$ increases as T_R increases, as predicted by eq 42 valid for $\Delta T \ll T_R$. Equation 46 also predicts that η^{el+ph}_{max} increases as $S^2\sigma$ decreases, indicating that a large value of the Seebeck coefficient is of critical importance for efficient thermoelectric refrigeration.

Figure 7(b) shows the numeric calculations of η_{el+ph} as a function of V_B for λ = 0, 1×10^{-17}, 3×10^{-17}, and 6×10^{-17} W/K^4, where ΔT = 1 K and T_R = 200 K. It shows that the upper limit of COP (η^{max}_{el+ph}) decreases as the strength of the phonon's thermal current increases because the phonon's thermal current is an adverse effect to refrigeration. Figure 7(b) also shows that the lower threshold bias $V^{th,lower}_{el+ph}$ increases as λ increases and agrees well with the prediction of eq 42.

In short, the phonon's thermal current, which is relevant to the mechanical coupling between the nanostructured object and the electrodes, is an adverse effect to refrigeration. To minimize the adverse effect, we suggest creating a weak mechanical link between the nanostructured object and the electrodes while still allowing electrons to tunnel.

III. D. Thermoelectric Cooling Effect Including the Phonon's Thermal Current and Local Heating. We further consider the effect of local heating on the thermoelectric refrigeration. Electrons that travel with energies larger than the

energy of normal modes can excite corresponding vibrations in the nanostructure anchoring the electrodes. This effect causes local heating in the nanostructure.[22−24] Local heating occurs when electrons exchange energy with the excitation and relaxation of the energy levels of the vibration of the nanostructured object that anchors the electrodes. The nano-object bridging the junction is formed by a few atoms, and thus the dispersion relation of the phonon is characterized by the lack of Goldstone mode. When normal coordinates are considered, the complex vibrations of a nano-object connecting to heavy electrodes can be cast into a set of independent simple harmonic oscillators described as normal modes. Due to the selection rule, the contributions to local heating from modes with large vibrational components along the direction of propagating electrons are important.[15] The smallest longitudinal normal mode has an energy of $eV_{onset} \approx 20$ meV.[69]

The heat generated in the central wire region can be dissipated to the bulk electrodes via phonon−phonon interactions. The heat generation eventually equilibrates the heat dissipation, where the wire region reaches an effective local temperature T_w higher than the averaged electrode temperatures $(T_L + T_R)/2$. Local temperature depends on several factors: the strength of coupling between electrons and the vibrations, the background temperature, and the mechanical coupling between the nanostructure and electrodes which determines the efficiency of the thermal current dissipating the thermal energy of local heating.

In Figure 8(a) we show the effective wire temperature (T_w) as a function of bias (V_B) for $T_R = 100$ and 300 K, where we assume that the strength of the phonon's thermal current is given by $\lambda = 1 \times 10^{-17}$ W/K^4. For $T_R = 100$ K, the increase of local wire temperature T_w is noticeable when $V_B > V_{onset} \approx 20$ mV. We note that T_w is slightly higher than T_R when $V_B < V_{onset}$ because only a small portion of electrons has energy larger than eV_{onset} due to the tail of the Fermi−Dirac distributions at finite temperatures. For $T_R = 300$ K, the increase in local wire temperature T_w is significantly suppressed due to increasingly efficient heat dissipation at high temperatures. The local heating generated in the wire region is dissipated to the left (hot) and right (cold) electrodes as described in eqs 54 and 55, respectively. The combined thermal current including the effect of the phonon's thermal current and local heating $(J^R_{el+ph+heating})$ is given by eq 57.

In Figure 8(b) we show the rate of local heating energy which is dissipated to the cold (right) electrode $(J^R_{local\ heating})$ as a function of bias (V_B) for $T_R = 100$, 200, 250, 300, and 350 K, where we assume that the strength of the phonon's thermal current is given by $\lambda = 1 \times 10^{-17}$ W/K^4. The rate of heating energy dissipated to the right (cold) electrode $(J^R_{local\ heating})$ introduces an additional negative effect to refrigeration, and thus, the combined thermal current $J^R_{el+ph+heating}$ which takes heat energy from the right (cold) reservoir to the left (hot) reservoir is suppressed. In this bias range, the heating power is smaller than 1% of the electric power (IV_B) supplied by a battery even at ambient temperatures because of the quasi-ballistic transport. This fact leads to $J^R_{local\ heating} \ll J^R_{ph}$ in the range of working biases $(V^{th,lower}_{el+ph} < V_B < V^{th,upper}_{el+ph})$ for the λ values we considered in this study. Consequently, the effect of local heating on thermoelectric refrigeration is negligible when the phonon's thermal current is included. This finding has profound implications on the design of the nanoscale thermoelectric refrigerator, where the local heating is strongly suppressed such that the overwhelming Joule heating in the bulk system can be avoided. This feature remarkably facilitates the electron cooling beyond the expectation of the conventional thermoelectric device theory.

We repeat the calculations in the previous two subsections. The results are not visibly different when we compare the ones that include contributions from both phonon's thermal current and local heating, as shown in Figure 4(c), Figure 5(c), Figure 6-(c), and Figure 7(c), with the ones that have phonon's thermal current only, as shown in Figure 4(b), Figure 5(b), Figure 6(b), and Figure 7(b).

IV. CONCLUSIONS

In summary, we propose a thermoelectric nanorefrigerator based on an atomic junction, the extreme limit of device minimization. In-depth research which combines the first-principles and analytical calculations is developed to study the thermoelectric cooling mechanism. The theory is applied to investigate the thermoelectric cooling of the 4-Al monatomic junction. The 4-Al junction is electronically simple such that the first-principle calculations reported here can be performed with a high level of accuracy. It, thus, serves as an ideal testbed for comparing the prediction of the theory and experiments. Our studies show that the P_x-P_y orbital characters near the chemical potential lead to a larger Seebeck coefficient in the 4-Al atomic junction. We investigated the working conditions, operation temperatures, electron's thermal current which removes heat from the cold temperature reservoir, and COP in the presence of the phonon's thermal current and local heating.

First, we perform first-principles calculations for the electron's thermal current (J^R_{el}) which removes heat from the cold temperature reservoir in the absence of the phonon's thermal current and local heating. The thermoelectric cooling is working when $J^R_{el} > 0$. It is observed that the operation of nanorefrigerators requires a minimum critical working temperature. The solution of $J^R_{el}(T_R) = 0$ defines the critical operation temperature denoted as T^{OP}_{el}. When $T_R < T^{OP}_{el}$, nanorefrigerators do not function. When $\Delta T = 0$, T^{OP}_{el} reaches the minimum value $(T^{OP}_{el})_{min}$, as given by eq 32. It is observed that the lowest critical operation temperature may be smaller than 100 K, which is very efficient as a low-temperature operated nanorefrigerator compared with the vacuum diode due to reduced work function via resonant tunneling. The working condition of the thermoelectric nanorefrigerator is quite demanding. The applied voltage is restricted to a small range of biases. It is observed that there are lower and upper bounds of biases denoted as V^{th}_{el} and $V^{th,upper}_{el}$, respectively. The thermoelectric nanorefrigerator does not work when the applied biases are smaller than V^{th}_{el} or larger than $V^{th,upper}_{el}$. Since the lower and upper threshold biases are small, it allows us to expand J^R_{el} and obtain an analytical expression for V^{th}_{el} and $V^{th,upper}_{el}$, as described in eqs 29 and 30. The maximum value of COP (η^{el}) occurs at bias around $2V^{th}_{el}$ and can be analytically expressed as eq 35.

Second, we consider the phonon's thermal current, which is a major effect against the operation of atomic refrigerators. To have a more perspective realization, we consider the phonon's thermal current in the approximation of the simplified weak-link model: $J^R_{ph} = \lambda(T^4_R - T^4_L)$. The simple model has a single parameter (λ) which allows us to construct an analytical theory to show the effect of the phonon's thermal current on electronic cooling in a transparent way. We choose λ around the order of 10^{-17} W/K^4 to present the effect of the phonon's thermal current. In this range of λ, the effect of the phonon's thermal current on the thermoelectric refrigeration is salient and

sensitive. In the presence of the phonon's thermal current, the combined thermal current (J^{R}_{el+ph}) which removes heat from the cold temperature reservoir decreases as λ increases. This leads to higher critical operation temperature T^{OP}_{el+ph}. The working conditions of the thermoelectric nanorefrigerator are hampered by the phonon's thermal current further, as described in eq 41. The range of biases which are allowed to drive nanorefrigerators shrinks. The lower bound of the operating bias (V^{th}_{el+ph}) increases as the intensity of the phonon's thermal current (λ) increases, as described in eq 42. The upper bound of the operating bias ($V^{th,upper}_{el+ph}$) decreases as λ increases. The COP (η_{el+ph}) is also suppressed by the intensity of the phonon's thermal current (λ) because the phonon's thermal current, taking heat from the hot to cold temperature reservoir, is an adverse effect to thermoelectric refrigeration. The suppression of the optimized COP (η^{max}_{el+ph}) by λ agrees well with the analytical expression given by eq 46. We would like to stress that the λ values chosen to present the strength of the phonon's thermal current is quite large. For example, the rate of thermal energy flows from electrode at 100 K to electrode at 0 K is 1 nW when $\lambda = 1 \times 10^{-17}$ W/K^4.

Third, we consider the effect of local heating on the thermoelectric refrigeration. Electrons that propagate with the energies larger than the energies of normal modes can excite corresponding vibrations in the nano-object anchoring the electrodes. This effect causes local heating in the nanostructure, which is analogous to Joule heating in the bulk system caused by diffusive electrons. The heat generated in the center region of the junction is dissipated to the hot and cold temperature reservoirs; and, thus, local heating is an adverse effect to electronic cooling. In the bulk system, irreversible Joule heating is overwhelming such that the efficiency of a thermoelectric refrigerator is significantly suppressed. Fortunately, the quasi-ballistic nature of electron transport in the atomic scale junctions significantly reduces local heating due the size reduction. This quantum feature remarkably facilitates thermoelectric cooling beyond the expectation of the conventional thermoelectric device theory. To demonstrate this point, we perform first-principles calculations for local heating using the Fermi golden rule in the first-order perturbation theory in the framework of density functional theory. Our calculations show that local heating dissipated to the cold temperature reservoir is very small compared with the large phonon's thermal current considered in this study. Consequently, local heating is negligible, especially in the small bias regime where the nanorefrigerant is functioning. Moreover, the photon radiation is also negligible even when we consider the perfect blackbody radiation for a nanojunction with a surface area of 1 μm diameter compared with the large phonon's thermal current.

Finally, we would like to mention that the simplified weak link model may not be perfect in a quantitative description of the phonon's thermal current. For example, it is valid only when $T \ll T_D$, where $T_D = 394$ K is the Debye temperature for Al. The value of $\lambda \approx 2\pi^5 K^2 C^2 k_B^4/(15)$ is unknown due to the uncertainty of the stiffness K of the bridging nano-object. For the 4-Al monatomic junction, $\lambda \approx 5.7 \times 10^{-15}$ W/K^4 where $K \approx 90.91$ N/m is obtained from total energy calculations and $C \approx 7.62 \times 10^8$ cm^2/erg^2 is obtained from the surface phonon dispersion relation from electronic-structure calculations. This λ value is considerably larger than the Pt monatomic chains with λ ranging from 0 to 2.05×10^{-19} W/K^4, where $K = 01261.2$ N/m is obtained from the experiments and $C = 1.887 \times 10^8$ cm^2/erg^2 is obtained from the surface phonon dispersion relation of Pt. The reason for the large discrepancy between the λ value is as follows: the stiffness of a 4-Al linear atomic chain ($K = 90.91$ N/m) from total energy calculations is much larger than the stiffness of a Pt monatomic chain ($K = 01261.2$ N/m) measured in experiments. This comparison infers that the stiffness K is likely to depend strongly on the detailed atomic structure of the full system, especially in the contact region. For example, the atom chain could be particularly stiff along the chain direction when the atomic chain forms a perfectly straight line; otherwise, the atomic (zigzag) chain could easily bend with much smaller stiffness. The total energy calculations have assumed that the atomic chain is perfectly linear. This may lead to significant overestimation for the λ value. The imperfection of the contact region in the real system may allow the possibility (for example, zigzag chain instead of perfect linear chain) to suppress the phonon's thermal current by creating a frustration in the mechanical link connecting to the electrodes. In this case, the thermoelectric refrigeration at an atomic scale may be salient.

In short, atomic-level control of the contact region is expected to open new opportunities and challenges in developing new forms of thermoelectric energy conversion devices. Atomic scale thermoelectric devices need to be extended by the utilization of unprecedented experiments. The nanorefrigerators potentially have better performance than the conventional TE refrigerators with the same ZT. The is due to the suppression of local heating and photon radiation due to the small size, which avoid the overwhelming Joule heating in the bulk system. This feature remarkably facilitates the electron cooling beyond the expectation of the conventional thermoelectric device theory.

AUTHOR INFORMATION

Corresponding Author

*E-mail: yuchangchen@mail.nctu.edu.tw.

ACKNOWLEDGMENT

The authors thank MOE ATU, NCHC, National Center for Theoretical Sciences (South), and NSC (Taiwan) for support under Grants NSC 97-2112-M-009-011-MY3, 098-2811-M-009-021, and 97-2120-M-009-005.

REFERENCES

(1) Aviram, A.; Ratner, M. A. *Chem. Phys. Lett.* **1974**, *29*, 277.
(2) Di Ventra, M. *Electrical transport in nanoscale systems*; Cambridge University Press: Cambridge, 2008.
(3) Kaun, C. C.; Guo, H. *Nano Lett.* **2003**, *3*, 1521.
(4) Di Ventra, M.; Lang, N. D. *Phys. Rev. B* **2001**, *65*, 045402.
(5) Nitzan, A.; Ratner, M. A. *Science* **2003**, *300*, 1384.
(6) Kamenetska, M.; Quek, S. Y.; Whalley, A. C.; Steigerwald, M. L.; Choi, H. J.; Louie, S. G.; Nuckolls, C.; Hybertsen, M. S.; Neaton, J. B.; Venkataraman, L. *J. Am. Chem. Soc.* **2010**, *132*, 6817.
(7) Solomon, G. C.; Herrmann, C.; Hansen, T.; Mujica, V.; Ratner, M. A. *Nature Chem.* **2010**, *2*, 223.
(8) Wang, W.; Lee, T.; Kretzschmar, I.; Read, M. A. *Nano Lett.* **2004**, *4*, 643.
(9) Galperin, M.; Nitzan, A.; Ratner, M. A. *Phys. Rev. B* **2008**, *78*, 125320.
(10) Jiang, J.; Kula, M.; Lu, W.; Luo, Y. *Nano Lett.* **2005**, *5*, 1551.
(11) Yu, L. H.; Zangmeister, C. D.; Kushmerick, J. G. *Phys. Rev. Lett.* **2007**, *98*, 206803.
(12) Paulsson, M.; Frederiksen, T.; Brandbyge, M. *Nano Lett.* **2006**, *6*, 258.
(13) Slomon, G. C.; Gagliardi, A.; Pecchia, A.; Frauenheim, T.; Di Carlo, A.; Reimers, J. R.; Noel, N. S. *J. Chem. Phys.* **2006**, *124*, 094704.

(14) Chen, Y. C.; Zwolak, M.; Di Ventra, M. *Nano Lett.* **2005**, *5*, 621.
(15) Chen, Y. C. *Phys. Rev. B* **2008**, *78*, 233310.
(16) Kristensen, I. S.; Paulsson, M.; Thygesen, K. S.; Jacobsen, K. W. *Phys. Rev. B* **2009**, *79*, 235411.
(17) Djukic, D.; van Ruitenbeek, J. M. *Nano Lett.* **2006**, *6*, 789.
(18) Kiguchi, M.; Tal, O.; Wohlthat, S.; Pauly, F.; Krieger, M.; Djukic, D.; Cuevas, J. C.; van Ruitenbeek, J. M. *Phys. Rev. Lett.* **2008**, *101*, 046801.
(19) Wheeler, P. J.; Russom, J. N.; Evans, K.; King, N. S.; Natelson, D. *Nano Lett.* **2010**, *10*, 1287.
(20) Chen, Y. C.; Di Ventra, M. *Phys. Rev. Lett.* **2005**, *95*, 166802.
(21) Liu, Y. S.; Chen, Y. C. *Phys. Rev. B* **2011**, *83*, 035401.
(22) Chen, Y. C.; Zwolak, M.; Di Ventra, M. *Nano Lett.* **2003**, *3*, 1691.
(23) Frederiksen, T.; Brandbyge, M.; Lorente, N.; Jauho, A.-P. *Phys. Rev. Lett.* **2004**, *93*, 256601.
(24) Huang, Z.; Xu, B.; Chen, Y. C.; Di Ventra, M.; Tao, N. J. *Nano Lett.* **2006**, *6*, 1240.
(25) Di Ventra, M.; Pantelides, S. T.; Lang, N. D. *Appl. Phys. Lett.* **2000**, *76*, 3448.
(26) Ma, C. L.; Nghiem, D.; Chen, Y. C. *Appl. Phys. Lett.* **2008**, *93*, 222111.
(27) Solomon, P. M.; Lang, N. D. *ACS Nano* **2008**, *2*, 435.
(28) Lang, N. D.; Solomon, P. M. *ACS Nano* **2009**, *3*, 1437.
(29) Song, H.; Kim, Y.; Jang, Y. H.; Jeong, H.; Reed, M. A.; Lee, T. *Nature* **2009**, *462*, 1039.
(30) Ahn, C. H.; Bhattacharya, A.; Di Ventra, M.; Eckstein, J. N.; Frisbie, C. D.; Gershenson, M. E.; Goldman, A. M.; Inoue, I. H.; Mannhart, J; Millis, A. J.; Morpurgo, A. F.; Natelson, D.; Triscone, J. M. *Rev. Mod. Phys.* **2006**, *78*, 1185.
(31) Lindsay, S. M.; Ratner, M. A. *Adv. Mater.* **2007**, *19*, 23.
(32) Tao, N. J. *Nat. Nanotechnol.* **2006**, *1*, 173.
(33) Ludoph, B.; van Ruitenbeek, J. M. *Phys. Rev. B* **1999**, *59*, 12290.
(34) Reddy, P.; Jang, S. Y.; Segalman, R. A.; Majumdar, A. *Science* **2007**, *315*, 1568.
(35) Baheti, K.; Malen, J. A.; Doak, P.; Reddy, P.; Jang, S. Y.; Tilley, T. D.; Majumdar, A.; Segalman, R. A. *Nano Lett.* **2008**, *8*, 715.
(36) Malen, J. A.; Doak, P.; Baheti, K.; Tilley, T. D.; Segalman, R. A.; Majumdar, A. *Nano Lett.* **2009**, *9*, 1164.
(37) Malen, J. A.; Yee, S. K.; Majumdar, A.; Swgalman, R. A. *Chem. Phys. Lett.* **2010**, *491*, 109.
(38) Paulsson, M.; Datta, S. *Phys. Rev. B* **2003**, *67*, 241403 (R).
(39) Zheng, X.; Zheng, W.; Wei, Y.; Zeng, Z.; Wang, J. *J. Chem. Phys.* **2004**, *121*, 8537.
(40) Wang, B.; Xing, Y.; Wan, L.; Wei, Y.; Wang, J. *Phys. Rev. B* **2005**, *71*, 233406.
(41) Pauly, F.; Viljas, J. K.; Cuevas, J. C. *Phys. Rev. B* **2008**, *78*, 035315.
(42) Galperin, M.; Nitzan, A.; Ratner, M. A. *Mol. Phys.* **2008**, *106*, 397.
(43) Dubi, Y.; Di Ventra, M. *Nano Lett.* **2009**, *9*, 97.
(44) Markussen, T.; Jauho, A. P.; Brandbyge, M. *Phys. Rev. Lett.* **2009**, *103*, 055502.
(45) Ke, S. H.; Yang, W.; Curtarolo, S.; Baranger, H. U. *Nano Lett.* **2009**, *9*, 1011.
(46) Finch, C. M.; Garca-Suárez, V. M.; Lambert, C. J. *Phys. Rev. B* **2009**, *79*, 033405.
(47) Markussen, T.; Jauho, A. P.; Brandbyge, M. *Phys. Rev. B* **2009**, *79*, 035415.
(48) Segal, D. *Phys. Rev. B* **2005**, *72*, 165426.
(49) Bergfield, J. P.; Stafford, C. A. *Nano Lett.* **2009**, *9*, 3072.
(50) Liu, Y. S.; Chen, Y. C. *Phys. Rev. B* **2009**, *79*, 193101.
(51) Liu, Y. S.; Chen, Y. R.; Chen, Y. C. *ACS Nano* **2009**, *3*, 3497.
(52) Hsu, B. C.; Liu, Y. S.; Lin, S. H.; Chen, Y. C. *Phys. Rev. B* **2011**, *83*, 041404 (R).
(53) Mahan, G. D. *J. Appl. Phys.* **1994**, *76*, 4362.
(54) Mahan, G. D.; Woods, L. M. *Phys. Rev. Lett.* **1998**, *80*, 4016.
(55) Chao, K. A.; Larsson, M.; Mal'shukov, A. G. *Appl. Phys. Lett.* **2005**, *87*, 022103.
(56) O'Dwyer, M. F.; Lewis, R. A.; Zhang, C.; Humphrey, T. E. *Phys. Rev. B* **2005**, *72*, 205330.
(57) Westover, T. L.; Fisher, T. S. *Phys. Rev. B* **2008**, *77*, 115426.
(58) D'Agosta, R.; Sai, Na.; Di Ventra, M. *Nano Lett.* **2006**, *6*, 2935.
(59) Huang, Z.; Chen, F.; D'Agosta, R.; Bennett, P. A.; Di Ventra, M.; Tao, N. J. *Nat. Nanotechnol.* **2007**, *2*, 698.
(60) Dubi, Y.; Di Ventra, M. *Phys. Rev. B* **2009**, *79*, 081302 (R).
(61) Galperin, M.; Saito, K.; Balatsky, A. V.; Nitzan, A. *Phys. Rev. B* **2009**, *80*, 115427.
(62) Segal, D. *Phys. Rev. Lett.* **2008**, *101*, 260601.
(63) Segal, D.; Nitzan, A. *Phys. Rev. E* **2006**, *73*, 026109.
(64) Liu, Y. S.; Yao, H. T.; Chen, Y. C. cond-mat/arXiv:1001.0822.
(65) Bergfield, J. P.; Solis, M. A.; Stafford, C. A. *ACS Nano* **2010**, *4*, 5314.
(66) Cuevas, J. C.; Levy Yeyati, A.; Martn-Rodero, A.; Bollinger, G. R.; Untiedt, C.; Agrat, N. *Phys. Rev. Lett.* **1998**, *81*, 2990.
(67) Thygesen, K. S.; Jacobsen, K. W. *Phys. Rev. Lett.* **2003**, *91*, 146801.
(68) Patton, K. R.; Geller, M. R. *Phys. Rev. B* **2001**, *64*, 155320.
(69) Yang, Z.; Chshiev, M.; Zwolak, M.; Chen, Y. C.; Di Ventra, M. *Phys. Rev. B* **2005**, *71*, 041402 (R).
(70) Shiota, T.; Mares, A. I.; Valkering, A. M. C.; Oosterkamp, T. H.; van Ruitenbeek, J. M. *Phys. Rev. B* **2008**, *77*, 125411.
(71) Kern, K.; David, R.; Palmer, R. L.; Comsa, G.; Rahman, T. S. *Phys. Rev. B* **1986**, *33*, 4334 (R).
(72) Chulkov, E. V.; Sklyadneva, I. Yu. *Surf. Sci.* **1995**, *331*, 1414.
(73) Lang, N. D. *Phys. Rev. B* **1995**, *52*, 5335.
(74) Chen, Y. C.; Di Ventra, M. *Phys. Rev. B* **2003**, *67*, 153304.